3-Minute Oscillations in the Upper Corona: Evidence from Parker Solar Probe

Zesen Huang (黄泽森) [ID],[1] Marco Velli [ID],[1] Chen Shi (时辰) [ID],[1] Yingjie Zhu (朱英杰) [ID],[2] B. D. G. Chandran [ID],[3] Victor Réville [ID],[4] Trevor Bowen [ID],[5] Nikos Sioulas [ID],[1] Marc Pulupa [ID],[5] Jia Huang (黄佳) [ID],[5] and Sheng Huang (黄胜) [ID][6]

[1]Department of Earth, Planetary, and Space Sciences, University of California, Los Angeles, CA, USA
[2]Physikalisch Meteorologische Observatorium, Davos, World Radiation Center (PMOD/WRC), 7260 Davos, Switzerland
[3]Space Science Center and Department of Physics, University of New Hampshire, Durham, NH 03824, USA
[4]IRAP, Université Toulouse III—Paul Sabatier, CNRS, CNES, Toulouse, France
[5]Space Sciences Laboratory, University of California, Berkeley, CA 94720-7450, USA
[6]Center for Space Physics, Boston University, Boston, MA, USA

ABSTRACT

Recent observations of Parker Solar Probe (PSP) from around the Alfvén surface have shown that the trace magnetic power spectrum density (PSD) is often characterized by a shallow-inertial double power law, where in the low frequency energy injection range, the power spectrum is shallow (flatter than $1/f$), and in the inertial range the spectrum is steep, with a scaling index of [1.5, 1.67]. Consequently, close to the sun, the majority of the fluctuation energy concentrates in a small frequency range around the low frequency power spectral break. In this work, we conduct a systematic survey of PSP observations for the first 17 encounters to statistically study the energy behaviors of the magnetic fluctuations. Our results show that the center frequency of fluctuation energy systematically drifts to around 3-minute for the most pristine solar wind (smallest solar wind advection time). Moreover, the center frequency rapidly drifts to lower frequency as solar wind advection time increases, as expected for active turbulence. The concentration of fluctuation energy around 3-minutes suggests that Alfvénic fluctuations in solar wind might mostly be coming from resonant p-mode oscillations in the photosphere, though other potential sources are discussed.

Keywords: Solar Wind, Helioseismology, Coronal Heating, Turbulence

1. INTRODUCTION

The heliosphere is created by the supersonic plasma flow originating from the Sun known as the solar wind. Parker (Parker 1958) successfully predicted the existence of the supersonic wind, which was later confirmed by *in situ* observations from the Luna 2 (Gringauz et al. 1962) and Mariner II spacecraft (Neugebauer & Snyder 1966). However, it was quickly realized (Parker 1965) that thermal conduction is not capable of accelerating the solar wind to high speed ($\gtrsim$ 700 km/s, see e.g. observations from Ulysses McComas et al. (2000)), and therefore additional injection of momentum and energy at substantial distances from the sun are necessary to heat and accelerate fast solar wind streams(Leer & Holzer 1980).

Large amplitude Alfvén waves are ubiquitous in the solar wind (Unti & Neugebauer 1968; Belcher & Davis 1971). Interplanetary Alfvénic fluctuations are characterized by a quasi-constant magnetic magnitude $|B|$,

hence the magnetic field vector tip appears to undergo a random walk on a sphere (Barnes & Hollweg 1974; Tsurutani et al. 1997; Matteini et al. 2014, 2024). Constant $|B|$ states are an exact solution of the Magnetohydrodynamics (MHD) equations, and can propagate without much damping. Consequently, Alfvénic fluctuations are considered to be a prime candidate for the heating and acceleration of the solar wind (Belcher 1971; Belcher & Olbert 1975; Alazraki & Couturier 1971; Hansteen & Velli 2012; Shi et al. 2022a)).

The origin of Alfvénic fluctuations in the solar wind remains debated. It has been conjectured that they may be generated by magnetic reconnection in the lower solar corona (Bale et al. 2021; Drake et al. 2021; Bale et al. 2023); others argue that Alfvén waves originate deeper in the solar atmosphere (Jess et al. 2009, 2015; Morton et al. 2023): either from the transition region and chromosphere (Tian et al. 2014; De Pontieu et al. 2007; Kuridze & Zaqarashvili 2008), or directly from

the photosphere where they are generated by convective motions (Cally 2012; Hansen & Cally 2012; Morton et al. 2013; Cally 2017; Morton et al. 2019; Kuniyoshi et al. 2023) or motions and shocks associated with G-band bright points (Cranmer & Ballegooijen 2005). It is well-known that the solar convection zone acts as a resonance chamber and the resultant fluctuations concentrate around 5-minute frequency, known as the p-mode (pressure-mode) oscillations (Ulrich 1970; Foukal 2004). In the chromosphere, the primary fluctuation frequency drifts slightly higher becoming the well studied chromospheric 3-minute oscillations (Fleck & Schmitz 1991; Jess et al. 2012). Entering the upper chromosphere and transition region, the primary fluctuation frequency can become larger but the measured values, between around 100-500s, are still debated (De Pontieu et al. 2007; Morton et al. 2012). In addition, higher frequency waves, known as decayless oscillations, are observed in coronal loops (Mandal et al. 2022; Zhong et al. 2023; Shrivastav et al. 2023). For recent reviews, see (Mathioudakis et al. 2013; Van Doorsselaere et al. 2020; Banerjee et al. 2021). It is therefore of interest to examine whether in-situ observations provide any evidence of fluctuation energy concentration in a certain range of frequencies in the upper corona.

Parker Solar Probe (PSP), launched in late 2018 (Fox et al. 2016), has been providing observations of the outer corona and inner heliosphere since 2021 (Kasper et al. 2021). The unprecedented *in situ* measurements close to the sun has ushered in a new era of space plasma studies (see e.g. Chen et al. (2020); Adhikari et al. (2020); Shi et al. (2021); Matthaeus (2021); Sioulas et al. (2022); Zank et al. (2022); Chen (2022); Zhang et al. (2022); Sioulas et al. (2023a,b); Dunn et al. (2023); Larosa et al. (2023); McIntyre et al. (2023), and see Raouafi et al. (2023) for a recent review). Notably, new observations from PSP have shown that the $1/f$ range in standard solar wind turbulence model (Bruno & Carbone 2013) appears to be absent closer to the sun, and instead shallower ($\sim f^{-0.5}$) spectra are found around the Alfvén surface, the region (that may look more like a thin shell due to its non-smooth behaviour) where the solar wind spead overtakes the Alfvén speed. It has been statistically evidenced that the $1/f$ range forms dynamically around 0.2 AU (Huang et al. 2023b; Davis et al. 2023; Chandran 2018). The $1/f$ range is also known as the energy containing range because the integrated fluctuation energy $\ln(f_2/f_1)$ depends only on the size of the frequency range, with each logarithmic interval containing the same energy. However, for the flatter spectra closer to the sun, the majority of the solar wind turbulence energy concentrates in a small range of frequencies

around the "bend" between the shallow low frequency range ($\sim f^{-0.5}$) and the inertial range ($\sim f^{[-1.67, -1.5]}$, see e.g. Chen et al. (2020); Sioulas et al. (2023b); McIntyre et al. (2023)).

Because the fluctuations in the solar wind turbulence are dominated by outwardly propagating modes it is reasonable to assume their launch to be found in the corona or deeper in the solar atmosphere, where the mean plasma flow is small (though this is not universally accepted). If this is correct, the frequency power spectrum measured by PSP can be associated with the real frequency spectrum launched at the base of the corona, subsequently modified by interactions with both the mean fields throught their gradients as well as nonlinear interactions. There is a Doppler shift resulting from the relative motion between the spacecraft and the solar wind (the radial Doppler shift can be considered negligible because $V_{psp,r} \lesssim 100$ km/s at perihelia, and the phase velocity of outward propagating Alfvén waves $V_{phase} = V_A + V_{SW} \sim 1000$ km/s $\gg V_{psp,r}$, but the perpendicular doppler shift could contaminate the frequency spectrum at perihelion. For a detailed discussion, refer to the appendix). As a result, the frequency of the "bend", i.e. the center frequency of the fluctuation energy f_{mid}, can be considered a proxy of the primary fluctuation frequency at the source (coronal base or deeper), if one assumes such frequency not to be significantly altered by nonlinear interactions (which however is subject to future scrutiny). In this study, we report the first *in situ* observational evidence that the magnetic fluctuation energy in upper solar corona universally concentrates around 3-minute. The rest of the paper is organized as follows: In the next section, we introduce the data and the relevant statistical methods; In section 3, we report the primary statistical results of center fluctuation frequency f_{mid} as a function of solar wind advection time $\tau_{adv} = (R - R_\odot)/V_r$; In section 4, we discuss the source of the Alfvén waves and the turbulence properties; In section 5, we conclude and summarize our results.

2. DATA AND METHODS

The magnetic field data is obtained from the fluxgate magnetometer in the FIELDS instrument suite (Bale et al. 2016) and the plasma measurements are acquired from the Faraday cup (SPC) and SPAN-ion from the SWEAP instrument suite (Kasper et al. 2019). Electron density data compiled from Quasi-Thermal-Noise (QTN) (Kruparova et al. 2023) is used as a proxy for proton density in the solar wind.

An example interval is shown in Figure 1. The trace power spectrum density (PSD_{FFT}) of magnetic field is
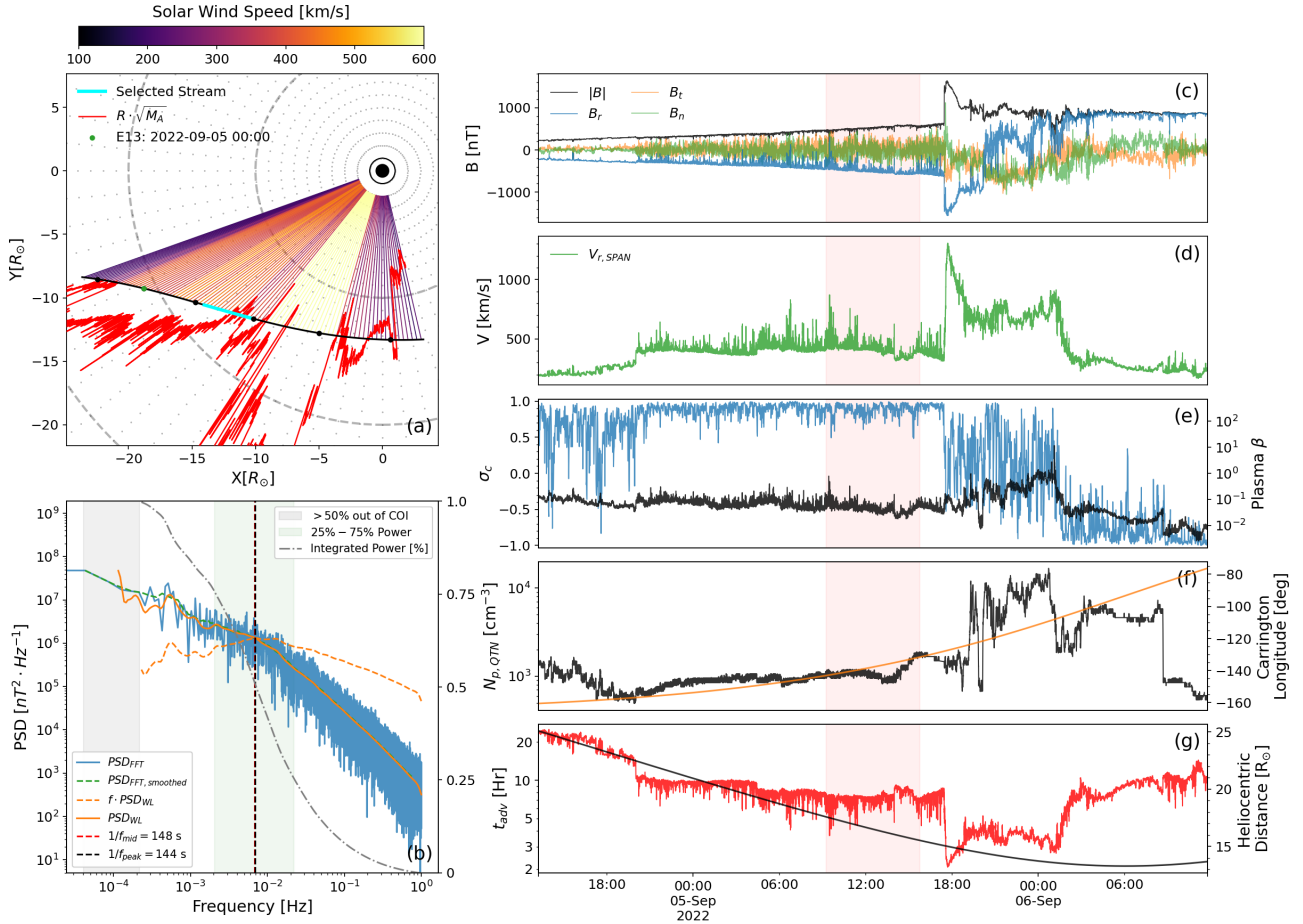
Figure 1. (a) Trajectory of PSP in the solar corotating frame with radial lines colored with local 10-minute average of solar wind speed. Black dots are plotted every 8 hours and the green dot indicates the entering direction. The red line is an illustration of the Alfvén mach number $M_A = V_r/V_A$. If the wind is super-Alfvénic, the red line falls out of the spacecraft trajectory (black line), and falls below the trajectory if the wind is sub-Alfvénic. The selected interval is highlighted with the cyan bar. (b) Trace magnetic power spectrum density (PSD) of the selected interval compiled from various methods. Blue: Fast Fourier Transformation (PSD_{FFT}). Green dashed: smoothed PSD_{FFT}. Orange: Wavelet Transformation (PSD_{WL}). Orange dashed: PSD_{WL} compensated with reference spectrum $1/f$. Gray area: frequency range where more than 50% of points fall out of the Cone of Influence (CoI) of the wavelet transformation (i.e. with too strong boundary effects). Dotted-dashed: Normalized integration of PSD_{WL} (orange line), i.e. normalized fluctuation energy, twin y-axis. Green area: frequency range over which the normalized fluctuation energy grows from 25% to 75%. Vertical dark dashed: middle frequency of the green area. Vertical red dashed: peak frequency of the compensated PSD_{WL} (orange dashed line). (c) R, T, N components and magnitude of the magnetic field. The selected interval is highlighted with the vertical pink area. (d) Radial solar wind speed from SPAN-ion and Alfvén speed $V_A = |B|/\sqrt{n_p m_p \mu_0}$. Proton density n_p is acquired from electron density from quasi-thermal-noise, and alpha particle and other heavier elements composition are ignored. (e) Cross helicity σ_c (left, blue) and plasma $\beta = 2\mu_0 P/B^2$ (right, black). (f) Proton density n_p (left, black) and Carrington Longitude (right, orange) (g) Advection time $\tau_{adv} = (R - R_\odot)/V_r$ (left, red) and Helio-radial distance R of the spacecraft (right, black).

shown in panel (b) in blue. The PSD is the trace sum of the squared amplitudes of the Fast Fourier Transformation (FFT) of the three magnetic vector components. To obtain a smoother spectrum, the PSD is smoothed using a window with a frequency factor of 2, and is shown in the green dashed line (sm-PSD_{FFT}). However, due to the rapid movement of PSP, the time series is naturally non-stationary, violating the fundamental assumptions of Fourier Transformation. Therefore, wavelet transfor-

mation is compiled for comparison, which is shown as orange line (PSD_{WL}). In general, we found that for frequencies where more than 50% of the PSD_{WL} falls within the Cone of Influence (CoI, shown as the gray shaded area), the PSD_{WL} and sm-PSD_{FFT} overlap almost perfectly with each other, and hence we entrust the overlapping frequency range. In this study, we consider the PSD_{WL} outside of the CoI range (part of the orange line that is outside of the gray area in panel (b))
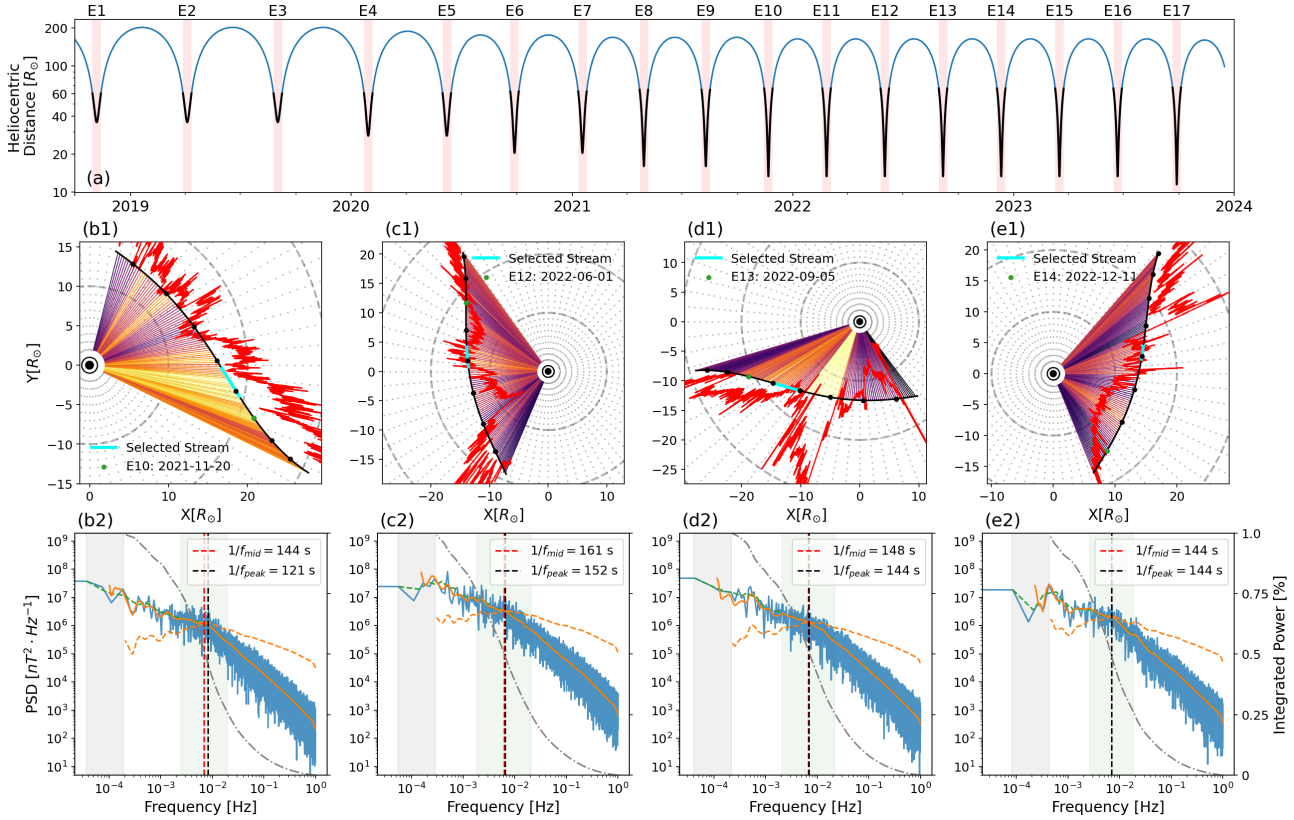
Figure 2. (a) Helio-radial distance of PSP by the end of 2023. The intervals considered in this study are highlighted with the black lines. (b1-e1) Trajectory of PSP (black line), Selected interval (cyan bar), Solar wind speed (colored radial lines), Illustration of Alfvén Mach number M_A ($R \cdot \sqrt{M_A}$, R is the radial distance of PSP, red line). Black dots are plotted every 8 hours and the green dot indicates the entering direction. (b2-e2) Trace magnetic power spectrum density (PSD) compiled from various methods: FFT (blue), smoothed FFT (green dashed), wavelet (orange), wavelet compensated with $1/f$ (orange dashed). Gray area: frequency range ignored due to Cone of influence. Green area: frequency range over which 50% (from 25% to 75%) of fluctuation energy resides. Red dashed: center of the green area. Black dashed: peak of the orange dashed line. Refer to Figure 1 for a colorbar for solar wind speed and detailed explanation for various lines.

as the primary power spectrum density of the magnetic field, and will henceforth refer to PSD_{WL} as PSD for simplicity. For detailed discussion of CoI, please refer to Huang et al. (2023b).

The normalized integrated power of the PSD is shown with the dashed-dotted line in the twin axis. The frequency range that contains 50% (from 25% to 75%) of the total fluctuation energy is highlighted with the green shaded area, and the center of the frequency range f_{mid} is shown with the red dashed line ($1/f_{mid} = 148s$). If the PSD scales as $1/f$, the energy distribution is independent of the specific frequency considered because the integrated power from f_1 to f_2 is $\ln(f_2/f_1)$. As a result, $1/f$ is the *de facto* "unity" reference spectrum, i.e. if the spectrum is steeper than $1/f$, the energy concentrate at the low frequency end, whereas if the spectrum is shallower than $1/f$, the energy concentrate at the high frequency end. Huang et al. (2023b) has shown that, close to the sun, the PSD is characterized by a double power

law where the low frequency range is shallower than $1/f$, and the inertial range is steeper, similar to Figure 1(b). Therefore, we compensate the spectrum with f, and the resultant compensated spectrum is shown with the orange dashed line. The compensated spectrum obviously shows a peak ($1/f_{peak} = 144s$), and we consider this as the "peak" frequency of the PSD, or the real location of the "bend".

Traditionally, the location of the low frequency spectral break is obtained from power law fit on both ranges of the PSD (see e.g. Bruno & Carbone (2013) and references therein). However, the turbulence spectrum measured by PSP close the sun (shallow-inertial) differ significantly from standard turbulence model ($1/f$-inertial), and sometimes displays a triple power law (shallow-$1/f$-inertial). Consequently, obtaining the low frequency spectral break locations from power law fits is highly unreliable. Thus we consider the f_{mid} defined above as a proxy to the low frequency spectral break,

which turns out to be surprisingly accurate when the spectrum has a shallow-inertial double power law.

In this study, we systematically surveyed the *in situ* solar wind time series from ± 7 days around the first 17 perihelia and they are summarized in Figure 2(a). We scan the date ranges with fixed window sizes of 2Hr, 3Hr, 4Hr, 6Hr, 8Hr and 12 Hr, with a fixed step size of 15-minute. We compile the wavelet PSD for each of the intervals, and calculate the center frequency of the frequency range where 50% of fluctuation energy resides (f_{mid}). We also calculate the averaged properties for each interval, including the mean solar wind speed, Alfvén mach number, and advection time ($\tau_{adv} = (R - R_\odot)/V_r$, R is the heliocentric distance of PSP, and V_r is the local radial solar wind speed). Whenever possible, we prioritize using V_r from SPAN-ion and electron density from QTN as a proxy for proton density due to the limited field of view of both SPAN-ion and SPC. Moreover, to better understand the radial evolution, we also focused on two extended intervals from inbounds of E10 and E12 that have been confirmed to be originated from single mid-latitude coronal holes (Badman et al. 2023; Huang et al. 2023c). Additionally, Huang et al. (2023c) has shown that the Gaussianity of $|B|$ can be used as a simple indicator for the wind originated from coronal holes, and hence a strong correlation to the Alfvénicity of solar wind. Therefore, in this study, besides an unbiased statistical survey, we also apply a simple threshold of Jensen Shannon Distance (JSD) smaller than 0.1 to filter the intervals with high level of Gaussianity in $|B|$, and thereby with high level of Alfvénicity.

3. RESULTS

3.1. *Case Studies: Pristine Alfvénic Solar Wind*

Figure 1 shows an example interval from E13 where the PSD is characterized by a shallow-inertial double power law. This phenomenon is among one of the unexpected discoveries of PSP (Huang et al. 2023b; Davis et al. 2023) and differs significantly from the standard solar wind turbulence model where the inertial range ends with an energy containing $1/f$ range (see e.g. Bavassano et al. (1982); Denskat & Neubauer (1982); Burlaga & Goldstein (1984) and Bruno & Carbone (2013); Tu & Marsch (1995) for reviews). Because of the shallow-inertial double power law, the majority of the fluctuation energy (dotted-dashed line) concentrates around the low frequency spectral break (or "bend") at around $1/f_{mid} = 148s$.

This interval is typical and interesting because : 1. It is (accelerating) fast Alfvénic wind, and thus likely originated from coronal hole. This can be seen from panel

(d) that the baseline $V_r \gtrsim 450km/s$ and from panel (e) that the normalized cross helicity $\sigma_c \simeq 1$; 2. It sits right at the Alfvén surface where the Alfvén Mach number $M_A = V_r/V_A$ ($V_A = |B|/\sqrt{\mu_0 n_p m_p}$) become unity, and therefore PSP is making *in situ* measurements in the upper corona. This can be seen from panel (a) where the red line ($R \cdot \sqrt{M_A}$) crosses the spacecraft trajectory towards the end of the interval and from panel (d) where the Alfvén speed V_A passes the radial solar wind speed V_r; 3. The radial distance of this interval is $R \sim 17R_\odot$ with advection time $\tau_{adv} \lesssim 8Hr$, and if we consider the group velocity ($V_g = V_A + V_r \gtrsim 1000km/s$) of the Alfvén waves, the real propagation time $t_p \lesssim 3.1Hr$. Thus, this interval is one of the most pristine solar wind streams measured by PSP. Note that the primary physical carriers of the fluctuation energy in the temporal domain are the so-called magnetic switchbacks, i.e. large amplitude spherically polarized outward propagating Alfvén waves (Bale et al. 2019; Squire et al. 2020; Dudok de Wit et al. 2020; Shoda et al. 2021; Rasca et al. 2021; Mozer et al. 2021; Bale et al. 2023; Drake et al. 2021; Tenerani et al. 2021; Shi et al. 2022b; Huang et al. 2023a; Larosa et al. 2023; Toth et al. 2023; Jagarlamudi et al. 2023; Bizien et al. 2023). Due to the polarization and the unidirectional outward propagation, these waves are accompanied by radial jets on the order of local Alfvén speed (Matteini et al. 2014) shown in both panel (a) and panel (d).

Figure 2 panels (b-e) show three more typical cases from E10, E12 and E14 where the PSD is characterized by a shallow power law (panel (d) is almost identical to Figure 1). All cases are Alfvénic fast wind that have not been thoroughly accelerated and the selected streams sit right at the Alfvén surface. In addition, the "bend" frequencies, or the center frequencies ($1/f_{mid}$) for fluctuation energy all concentrate at around 3-minute. It should be noted here that the selected streams from panel (b) and (c) (E10 and E12) have been confirmed by previous studies using Potential Field Source Surface modeling (Badman et al. 2020; Panasenco et al. 2020) to both originate from single mid-latitude coronal hole (Badman et al. 2023; Huang et al. 2023c).

The cases shown above indicate that the fluctuation energy concentrates around 3-minute for the pristine Alfvénic solar wind. Notably, if one assumes the spacecraft remains stationary (see Appendix B for discussion of the doppler effects from PSP movement), and the time series are created solely by the advection of the solar wind, the frequency spectrum measured by PSP should be identical to the frequency spectrum at the source of the wind (corona base or deeper), provided that nonlinear effects are insignificant. Therefore, it is

6

of great interest to conduct a systematic survey for the statistical behaviors of magnetic fluctuations in the solar wind to study the radial evolution of $1/f_{mid}$. One may expect that $1/f_{mid}$ evolves towards 3-minute with decreasing advection time τ_{adv}.

3.2. Statistical Results: E1-E17

Figure 3 shows the statistical results of $1/f_{mid}$ from a systematic scan with 6-Hour fixed window and 15-minute step size of $\pm$ 7 days around the first 17 PSP perihelia. The intervals whose $\sigma_{\tau_{adv}}/\langle\tau_{adv}\rangle > 20\%$ are discarded (about 6.5% of all intervals), and we ends up with 20975 intervals. The results are presented as a function of advection time $\tau_{adv} = (R - R_\odot)/V_r$, where R is the mean heliocentric distance of each interval and V_r is the interval averaged radial solar wind speed. τ_{adv} can be considered as a proxy to the "age" of the solar wind plasma because the solar wind speed increases exponentially from corona base to the Alfvén surface. Panel (a) shows the statistics of all of the 20975 intervals. Evidently, $1/f_{mid}$ trends nicely with τ_{adv} and gradually stabilizes around 3-minute for the "youngest" solar wind. However the scatters are spread because the fixed 6 hour long window does not discriminate large scale structures in the solar wind like Heliospheric current sheet (HCS) crossings, Coronal Mass Ejections (CME) or ICME, and magnetic holes. Albeit being intrinsic components of the solar wind, these structures are usually not considered part of the solar wind turbulence. In order to better understand the radial evolution of f_{mid} for Alfvénic turbulence, it is beneficial to filter the Alfvénic wind.

Huang et al. (2023c) discovered a simple connection between the Gaussianity of magnetic magnitude $|B|$ and the coronal hole origin of the wind. High level of Gaussianity in $|B|$ indicates constancy of $|B|$ and hence high level of Alfvénicity. Based upon this simple relation, we select the intervals with highly Gaussian $|B|$ using the Jensen-Shannon Distance threshold of 0.1, and 6680 intervals survived. The statistical results of the filtered intervals are shown in panel (b). The filtered intervals are clearly more concentrated with the majority of the outliers removed (HCS crossing, CME and magnetic holes can significantly destroy the Gaussianity of $|B|$). Similarly, $1/f_{mid}$ stabilizes around 3-minute for the most pristine solar wind, and the binned mean line remains largely consistent. To better understand of radial evolution of $1/f_{mid}$ inside of coronal holes, the intervals from the two extended time range with confirmed mid-latitude coronal hole origin are highlighted (blue: E10, orange: E12). The points are connected with dashed lines based on their interval averaged heliocentric distance R to indicate the order of measurement. The

trend is clear: as τ_{adv} decreases, $1/f_{mid}$ gradually decrease until it saturates at 3-minute and stays around the saturation value even though the helio-radial distance R continue to decrease.

Additionally, τ_{adv} in fact significantly over-estimates the "age" of the Alfvén waves because from the energy perspective the "age" is determined by the integral of the group velocity from corona base to PSP. Adopting a typical Alfvén speed V_A and solar wind speed V_r profile, e.g. Figure 1 in Verdini et al. (2012), the group velocity in the frame of the static sun $V_g = V_A + V_r$ is almost always larger than $1000km/s$, translating to an "age" smaller than 2.01 hours for an interval measured at 11.4 $R_\odot$. Therefore, the "age" of the Alfvén waves is actually much younger than the τ_{adv} shown in Figure 3, especially for the intervals with small τ_{adv} values that are located on the left side of panels (a) and (b) whose Alfvén speed is comparable to solar wind speed. This has two major implications: 1. Future orbits of PSP can at best measure intervals with "age" $\simeq 1.72$ hours assuming perihelion distance $R = 9.9R_\odot$ and a mean group velocity of $V_g = 1000km/s$; 2. Referring to the evolution of $1/f_{mid}$ in Figure 3, a half-hour change in τ_{adv} makes marginal difference in $1/f_{mid}$. Therefore, our results are representative of the measurement limit in terms of PSP orbit design.

Notably, during the perihelion, the perpendicular speed of PSP can reach up to $V_{inertial,\phi} \simeq 200$km/s in the inertial frame and can reach up to $V_{carr,\phi} \simeq 100$km/s in the co-rotating frame. The Alfvén waves are guided by the background magnetic field, which is mostly radial around perihelion. For the solar wind plasma measured by PSP around perihelion, typically $|B|$ is quasi-constant ($\delta|B|/|B| \lesssim 0.01$), and plasma β is very small ($\beta < 0.1$). Consequently, in the MHD regime, there is no information carrier in the ϕ direction, and hence the perturbations can be considered causally unrelated. Adopting $V_\phi \simeq 100$km/s in the co-rotating frame, 3-minute can be translated into 18Mm at $12R_\odot$, and thus 1500km at the corona base assuming a radial expansion of the coronal hole flux tube. Using a modest super-radial expansion factor of 3 from photosphere to corona base, the physical size can be mapped to 500km at the photosphere, about 1/3 the size of the granule (for V_ϕ in the inertial frame, about 2/3 the size of a granule). Assuming that the perturbation as a function of perpendicular spatial coordinates can be written as power spectrum density with power law dependence $P(k_\phi) \propto k_\phi^{-\alpha}$, and $\alpha > 1$. In this scenario, the wave number spectrum can 'contaminate' the frequency spectrum via doppler shift:

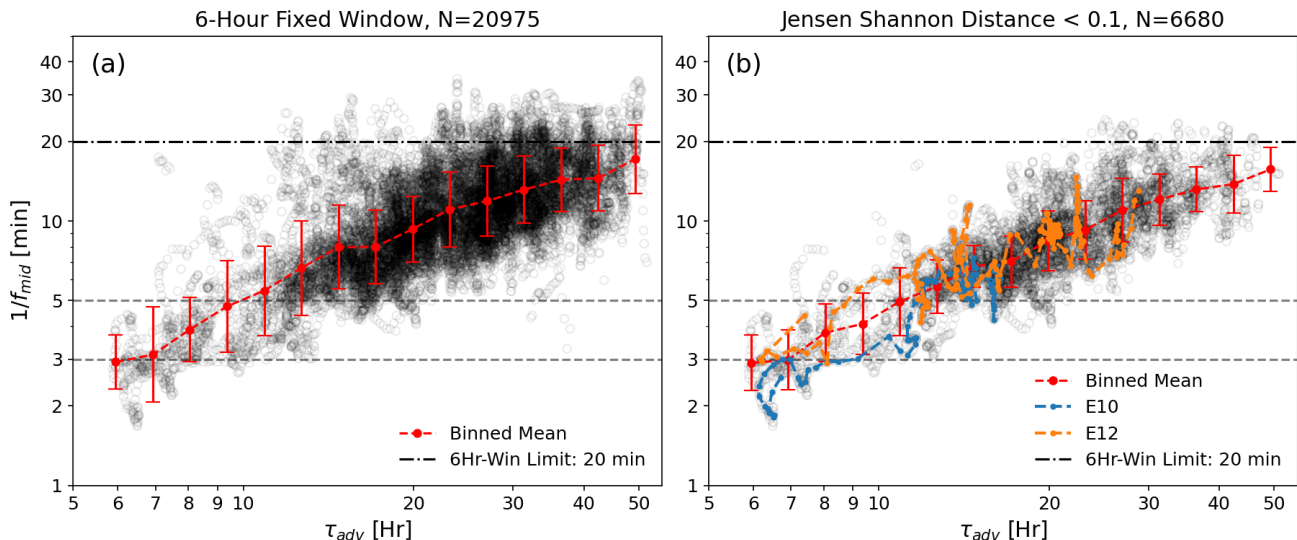$$2\pi f = k_\phi V_\phi \tag{1}$$

Figure 3. (a) Statistics of the center frequency of the fluctuation energy $1/f_{mid}$ of total 20975 intervals with fixed 6-hour window as a function of advection time $\tau_{adv} = (R - R_\odot)/V_r$, where V_r is the interval mean radial solar wind speed and R is the mean heliocentric distance of the interval. The red line is the binned mean of the scatters with errorbars indicating one standard deviation of the points within each bin. The dotted dashed line indicates the upper limit of $1/f_{mid}$ for the 6-hour window size assuming a Kolmogorov $f^{-5/3}$ spectrum. (b) Statistics of the 6680 intervals filtered with Jensen-Shannon Distance of $|B|$ smaller than 0.1, i.e. $|B|$ is highly Gaussian. This criterion filters out intervals with high level of Alfvénicity and indicates coronal hole origin of the streams. The radial evolution within two confirmed coronal holes from inbounds of E10 and E12 are highlighted with the blue and orange lines.

Due to the steep power law dependence ($\alpha > 1$), the 'contamination' becomes strongest when V_ϕ reaches its maximum right at the perihelion (for the same f, it corresponds to smaller k, and thus higher energy level). Even though we have no information on the $P(k_\phi)$ at the Alfvén surface, due to the causal independence of the perturbation in the ϕ direction, we can refer to the perpendicular spectrum in the photosphere. Based on Solar Optical Telescope observations (Rieutord et al. 2010), the perpendicular power spectrum density follows $P(k_\perp) \propto k_\perp^{-10/3}$ for the sub-granular scales, and reaches a peak at the Granulation scale of 1700 km. Due to the steepness of the spectrum, one would only expect strong 'contamination' in the frequency spectrum when V_ϕ is large. However, both $V_{inertial,\phi}$ and $V_{carr,\phi}$ changes significantly over a small range of radial distance around the perihelion. This could be the reason why we see a upper trend in $1/f_{mid}$ in Figure 5(b) as PSP approaches perihelion for both coronal hole intervals from inbounds of E10 and E12. Consequently, the real primary oscillation frequency in upper corona could be closer to 2-minute than 3-minute. Nevertheless, here we decided to present the original statistics for the sake of clearness and reproductivity. For more detailed discussion on the doppler shift, please refer to the appendix.

In summary, together with case studies and statistical scans, we have provided strong evidence that the magnetic fluctuation energy concentrates around 3-minute

for the most pristine solar wind that are measured *in situ* around the Alfvén surface.

4. DISCUSSION

4.1. *The Source of the Alfvén Waves*

A well-established physical picture of the source of the Alfvén waves in the corona (Morton et al. 2023) is that the fluctuations originate from the 5-minute p-mode (pressure-mode) in the photosphere where $\beta \gg 1$, i.e. sound speed c_s is much greater than Alfvén speed v_A. Going up into the middle of the chromosphere lies the magnetic canopy, i.e. layer where $c_s = v_A$ ($\beta \sim 1$, introduced by Rosenthal et al. (2002); Bogdan et al. (2003)), within which linear mode conversion between the two magnetosonic modes is possible. Below the canopy, $c_s > v_A$, the fast mode is sonic (compressive) and isotropic, and hence $\delta\vec{v} \parallel \vec{k}$, where $\delta\vec{v}$ is the velocity perturbation and $\vec{k}$ is the wave vector. On the contrary, the slow mode is magnetic and guided by the background magnetic field $\vec{B}_0$. In addition, due to the high β environment, the motion of the magnetic field lines are largely controlled by the plasma motion. On the other hand, above the canopy where $c_s < v_A$, the slow mode becomes the pure sonic mode but is highly anisotropic, i.e. guided by $\vec{B}_0$, and the fast mode is now magnetic and isotropic. Moreover, due to the low β environment, the plasma is being controlled by the magnetic field. Consequently, mode conversion from the sonic fluctua-

tions below the canopy (fast mode) to magnetic fluctuations above the canopy (fast mode) is possible when the eigen perturbation $\delta\vec{v}$ of both modes are not orthogonal. This linear mode conversion has been shown by numerous simulation studies (Spruit & Bogdan 1992; Cally & Bogdan 1997; Cally 2000; Crouch & Cally 2003; Bogdan et al. 2003), and has also recently shown that the mode conversion conserves wave action (Huang et al. 2022). Passing through the magnetic canopy, the fast magnetosonic mode will face a steep Alfvén speed profile and hence be refracted. Around the height of the refraction, the fast mode linearly couples with the Alfvén mode and is hence partially converted (Cally & Hansen 2011; Cally 2017; Khomenko & Cally 2019). The mode conversion from p-mode in the photosphere to Alfvén mode in the upper chromosphere and transition region is termed "double mode-conversion" (Khomenko & Cally 2012) and is expected to allow 30% of the p-mode flux to pass through the transition region carrying an energy flux of 800 Wm^{-2} in the 3-5 mHz frequency band (3-5 minutes) (Hansen & Cally 2012). 1D simulation from Réville et al. (2018) also indicates that for Alfvén wave with 3-minute period, the transmission coefficient through the transition layer is about 50%.

From the corona base to the spacecraft at Alfvén surface, one should be careful about the non-WKB effects of Alfvén wave due to steep Alfvén speed profile, i.e. reflection (Heinemann & Olbert 1980; Hollweg 1990; Velli et al. 1991; Velli 1993). Here we use a Heliosphere model which includes the transition from static atmosphere to propagating solar wind from Velli et al. (1991):

$$\rho = \rho_0 \frac{\exp\{-\alpha/2 \cdot [1 - (R_\odot/R)]\}}{\{1 + \beta[(R/R_\odot - 1)]\}^2} \quad (2)$$

$$V_a = V_{a0} \left(\frac{R_\odot}{R}\right)^2 \left(\frac{\rho_0}{\rho}\right)^{1/2} \quad (3)$$

$$U = \frac{U_\infty}{\beta^2} \exp(-\alpha/2) \left(\frac{R}{R_\odot}\right)^2 \left(\frac{V_a}{V_{a0}}\right)^2 \quad (4)$$

where V_{a0} is the initial Alfvén speed at the corona base, U_∞ is the asymptotic solar wind speed at infinity, and α and β are free parameters. To find a typical transmission coefficient for the 3-minute ($\simeq$5.5 mHz) wave, we adopt some reasonable values: $\alpha = 0, \beta = 5, V_{a0} = 2000$km/s, $U_\infty = 700$km/s, and this produces a Alfvén surface at a realistic distance of $15.09R_\odot$. Following Velli (1993), the transmission coefficient (with respect to the conserved wave action/quantum in the WKB limit) of frequency 5.5 mHz is calculated to be $T(5.5\text{mHz}) \approx 99.8\%$, which is effectively perfect transmission. One can of course play with different α, β, V_{a0} and U_∞, but as long as the parameters are consistent with realistic fast wind conditions, the trans-

mission coefficient for 5.5 mHz wave will be almost always close to 100%, i.e. very close to the ideal WKB range. Thus, as least within 1-D model, the 3-minute Alfvén wave can be safely considered as WKB from the corona base to Alfvén surface. In fact, as been discussed in Velli (1993), the existence of the wind can significantly increase the transmission for the low frequency waves, which are completely reflected otherwise, and the asymptotic transmission coefficient is:

$$T_c = \frac{4V_{A0}V_{Ac}}{(V_{A0} + V_{Ac})^2} \quad (5)$$

where V_{A0} is the Alfvén speed at the corona base and V_{Ac} is the Alfvén speed at the Alfvén critical surface. Consequently, the steep Alfvén speed profile from corona base to the Alfvén surface can at most insignificantly reflect the injected energy, if not negligibly. For more detailed discussions, please refer to the Appendix.

The concentration of turbulence fluctuation energy around 3-minute at the Alfvén surface and upper corona is therefore particularly interesting because it is not only in favor with the aforementioned Alfvén wave generation mechanisms, but is also compatible with various remote sensing observations made at lower corona (Morton et al. 2016, 2019, 2023), transition region (Tian et al. 2014), and chromosphere (De Pontieu et al. 2007). It is well known from observations that the fluctuations from below the transition region is strong enough to power the fast solar wind (which needs $\gtrsim 100W/m^2$) even assuming a weakest transmission coefficient of 3% at the transition layer (De Pontieu et al. 2007). Previous *in situ* studies of the solar wind turbulence on the energy injection range have predominantly shown that the low-frequency spectral breaks between the inertial range and $1/f$ range lie at very low frequencies ($\lesssim 10^{-3}Hz \sim 3Hr$, see e.g. Wu et al. (2020, 2021b); Bruno & Carbone (2013); Bruno et al. (2019); Bavassano et al. (1982); Denskat & Neubauer (1982); Burlaga & Goldstein (1984); Tu & Marsch (1995)), perhaps with only one exception from the single fast solar wind interval from Helios 2 (see Figure 1 in Wu et al. (2021a) and Figure 29 in Bruno & Carbone (2013)) where the low frequency spectral break occurred at around $10^{-2}Hz$. Note that this specific interval measured at 0.29AU has also been previously recognized and analyzed by Chandran (2018) from Fig 2-2(c) of Tu & Marsch (1995) as a shallow-inertial double power law, and in fact it is a very typical shallow-$1/f$-inertial triple power law. Nevertheless, it should be noted that the $1/f$ range indicates a scale-independent distribution of fluctuation energy, and hence the central frequency of fluctuation energy for that specific interval from Helios 2 is located at a much lower

frequency than the spectral break. Therefore, the existence of the shallow ($f^{-\alpha}, \alpha < 1$) and steep ($\alpha > 1$) double power law spectra that were first observed by PSP (Huang et al. 2023b; Davis et al. 2023) provide the first evidence that the Alfvén wave power concentrates around a specific small frequency range. The purpose of this study is to show it is statistically true that in the upper solar corona and around the Alfvén surface, the primary frequency of magnetic fluctuations concentrates around 3-minute, thereby consistent with both numerical modeling and remote sensing observations.

It should be noted, however, that, our results pose yet no preference for either of the two primary coronal heating mechanisms, i.e. AC (waves heating) and DC (reconnection/nano-flare heating) (see e.g. Hansteen & Leer (1995); McComas et al. (2007); Velli et al. (2015); Van Doorsselaere et al. (2020); Banerjee et al. (2021)). As been pointed out by Parker (1991), to maintain the million degree solar corona, much of the energy has to be deposited within the first few solar radii above the transition region. This is difficult for Alfvén waves due to their stability (see e.g. simulation by Tenerani et al. (2020)) as long as the background magnetic field structure is not complex. Our study can serve as an example for future studies to constrain the coronal heating mechanisms using *in situ* observations from PSP.

4.2. $1/f$ Range, Turbulence Cascade and Dissipation

Figure 3 also manifests an active turbulence cascade and dissipation. From both panels we see clear trends that f_{mid} moves to much lower frequency as the advection time increases (or as the solar wind grows "older"). However, the trend of f_{mid} with regard to τ_{adv} should be interpreted with caution because it is result of combination of multiple processes: 1. The energy containing $1/f$ range is being dynamically created as the radial distance of PSP increases (Huang et al. 2023b; Davis et al. 2023); 2. The active turbulence cascade and dissipation "eat-up" the energy containing range and move the low frequency spectral break between $1/f$ and inertial to low frequency (see models e.g. Tu & Marsch (1993, 1995) and observations (Bruno & Carbone 2013; Chen et al. 2020; Wu et al. 2021a; Sioulas et al. 2022)); 3. Our method of compiling f_{mid} using the normalized integrated energy curve can only capture the location of low frequency break when the spectrum has a clear shallow-inertial double power law (e.g. the four spectra in Figure 2). However it can not capture of the location of the low frequency spectral break when the spectrum becomes a triple power law (shallow-$1/f$-inertial) or the classical double power law ($1/f$-inertial), and it will instead produce a value with slightly lower frequency. All

of the aforementioned caveats will be obvious when one views a video of Figure 1 produced using a sliding window (see supplement materials).

The supplemental video therefore provide some evidence that the energy containing $1/f$ range is dynamically created after the solar wind leave the Alfvén surface and the fluctuation energy subsequently "spread-out" from its concentration around 3-minute, creating a triple power law (shallow-$1/f$-inertial). This phenomenon has been predicted based on a turbulence model (Chandran 2018) and been found in turbulence simulation (Meyrand et al. 2023). However, detailed discussion of the formation mechanism of $1/f$ range lies beyond the scope of this study and it is a topic of active debates (see e.g. Keshner (1982); Montroll & Shlesinger (1982); Bak et al. (1987); Velli et al. (1989); Matthaeus & Goldstein (1986); Matthaeus et al. (2007); Bemporad et al. (2008); Dmitruk et al. (2011); Verdini et al. (2012); Matteini et al. (2018); Chandran (2018); Magyar & Doorsselaere (2022); Meyrand et al. (2023)).

For completeness, here we provide an order of magnitude estimate of solar wind heating rate from our statistical results shown in Figure 3(a) using the equation (D24). We may assume that the low frequency spectrum scales like $1/f$ and the inertial range scales like $f^{-5/3}$ or $f^{-3/2}$ and hence $\alpha_0 = 1$ and $\alpha_1 = 5/3$. Adopting a typical spectrum intensity at the spectral break to be $C_0 f_c^{-\alpha_0} = (10^{-5} \text{ nT}^2 \cdot \text{Hz}^{-1})/\mu_0$, and the near sun change of f_c from panel (a) to be $df_c/dt = (1/3\text{min} - 1/6\text{min})/(12\text{Hr} - 7\text{Hr})$, finally the solar wind heating rate is estimated to be: $-\epsilon(t) \simeq 1.23 \times 10^{-14} \text{W} \cdot \text{m}^{-3}$. This value is consistent with the results from Wu et al. (2020).

5. SUMMARY AND CONCLUSION

In this study, we conducted a systematic survey of the solar wind magnetic fluctuations for the first 17 perihelia of PSP. Our results have shown that as PSP gets closer to the Alfvén surface, the turbulence power spectrum density (PSD) is often characterized by a shallow-inertial double power law: in the energy injection range, the spectrum is shallower than $1/f$, and in the inertial range, the spectrum is steeper than $1/f$. Consequently, the energy concentrates around the "bend" (low frequency power spectral break). This phenomenon differs significantly from traditional solar wind turbulence models, and shows strong indication that close to the sun (around the Alfvén surface), there exists a primary frequency for the magnetic fluctuations in the solar wind.

Our thorough scan of the data has shown that the primary frequency (or the center frequency of fluctuation power, f_{mid}) trends almost perfectly with advec-

tion time $\tau_{adv} = (R - R_\odot)/V_r$, where R is the heliocentric distance and V_r is the radial solar wind speed, and it stablizes at around 3-minute for the "youngest" solar wind streams, compatible with the famous chromospheric 3-minute oscillations, which is considered to be driven by the photosphere 5 minute p-mode oscillations. Therefore, our results provide a strong evidence that the fluctuations in the solar wind (whose primary physical carriers are the magnetic switchbacks, i.e. large amplitude spherically polarized outward propagating Alfvén waves) are sourced from the lower solar atmosphere, possibly ultimately driven by the resonance chamber on the sun.

Parker Solar Probe will enter its final orbits with perihelion at 9.86 $R_\odot$ in December 2024 amid the climax of solar cycle 25, and hence can potentially observe Alfvénic solar wind with $\tau_{adv} \lesssim 4Hr$ (assuming $R - R_\odot = 8.9R_\odot$ and $V_r \simeq 450km/s$). Future measurements may either provide stronger evidence that $1/f_{mid}$ actually stablizes at 3-minute or disprove it. Nevertheless, one should be reminded that $\tau_{adv} \simeq 6Hr$ is already extremely "young" for Alfvénic solar wind originating from coronal holes. Our results therefore serve as the first *in situ* evidence that there exists an energy concentration of magnetic fluctuations at around 3-minute frequency at around the Alfvén surface and in the upper solar corona.

APPENDIX

A. CASE LIST

Here we provide a list of cases where the trace magnetic PSD can be characterized by a clear shallow double power law and the center frequency of fluctuation energy $1/f_{mid} \simeq$ 3-minute. The "$1/f_{min}$" column indicates the minimum frequency in minutes considered trustworthy for each PSD, i.e. the right edge of the grey area in Figure 1(b). The "$\Delta\phi$" column lists the minimum and maximum angular velocity for each intervals times the "$1/f_{min}$", indicating the possible value range of Carrington longitude change for the lowest frequencies. The M_A column shows the interval averaged Alfvén mach number ($M_A = V_r/V_A$), where $M_A > 1$ indicates that PSP is in the solar wind and $M_A < 1$ indicates that PSP is inside of the solar corona. The "$1/f_{mid}$" column shows the middle frequency of the magnetic fluctuation energy defined in the main text.

#	Enc	Start	Size	$1/f_{min}$[min]	$\Delta\phi$[deg]	V_r[km/s]	$R[R_\odot]$	τ_{adv}[Hr]	M_A	$1/f_{mid}$[s]
1	10	2021-11-19 20:00	07:15	82.8	(0.80, 1.26)	541.58	22.00	7.55	1.54	186
2	10	2021-11-20 03:45	03:15	36.9	(0.58, 0.70)	545.93	19.82	6.74	1.44	148
3	10	2021-11-20 06:30	07:30	86.0	(1.59, 2.41)	537.39	18.06	6.20	1.37	144
4	10	2021-11-20 12:45	07:45	89.4	(2.35, 3.42)	460.93	15.97	6.34	1.20	136
5	10	2021-11-21 05:00	06:00	68.3	(3.39, 3.48)	421.17	13.30	5.75	1.05	161
6	11	2022-02-25 15:30	04:45	54.2	(2.64, 2.76)	378.80	13.36	6.45	0.79	161
7	11	2022-02-26 03:15	03:15	36.9	(1.24, 1.43)	371.27	15.25	7.64	1.04	132
8	12	2022-06-01 05:45	04:00	45.6	(1.37, 1.66)	344.98	15.75	8.31	0.60	161
9	12	2022-06-01 12:30	05:00	57.4	(2.35, 2.74)	418.20	14.02	6.08	0.87	161
10	13	2022-09-05 03:45	03:30	39.8	(0.72, 0.88)	442.01	18.90	7.91	1.30	157
11	13	2022-09-05 09:15	06:30	73.7	(1.82, 2.54)	410.37	16.51	7.36	0.93	148
12	13	2022-09-05 14:00	03:15	36.9	(1.17, 1.36)	368.76	15.57	7.70	0.97	128
13	14	2022-12-11 23:15	03:15	36.9	(1.34, 1.53)	362.07	14.82	7.45	0.85	144
14	15	2023-03-17 13:30	04:00	45.6	(2.09, 2.27)	427.18	13.59	5.74	0.98	136
15	15	2023-03-17 15:45	03:15	36.9	(1.78, 1.87)	411.73	13.41	5.93	0.94	124
16	15	2023-03-17 23:30	03:30	39.8	(1.86, 1.99)	403.94	13.56	6.21	0.90	152
17	15	2023-03-18 02:15	03:30	39.8	(1.70, 1.89)	337.81	13.96	7.48	0.86	144
18	16	2023-06-21 10:00	03:15	36.9	(1.07, 1.26)	241.82	16.07	12.29	1.19	144
19	16	2023-06-21 16:00	04:30	51.1	(1.97, 2.32)	281.35	14.34	9.28	1.02	161
20	17	2023-09-27 14:30	03:15	36.9	(1.91, 2.20)	352.44	12.31	6.33	0.92	114

B. INTERPRETATION OF TEMPORAL SIGNALS

The data provided by PSP are time series of different measurable quantities from single spacecraft measurements, such as vector magnetic field, vector proton velocities, proton densities, etc. Consequently, different studies interpret the raw temporal signals using different assumptions. Partially due to the predominant dependence on wavevector in most of the turbulence theories and models, a significant portion of the observational studies interpret the temporal signals as wind-advected spatial structures in order to make comparisons. To convert the temporal signals into spatial signals, Taylor Hypothesis (TH) Taylor (1938) is used:

$$k \cdot U = 2\pi f \tag{B1}$$

where k is the wavenumber, U is the local solar wind speed, and f is the given frequency from the observed data. k is considered created by the advection of the solar wind at speed U, and hence $\vec{k} \parallel \vec{U}$ locally. In addition, locally averaged

vector magnetic field $\langle\vec{B}\rangle$ is compiled at the given temporal window $1/f$ in a sliding window fashion to represent the local "parallel" direction in the turbulence anisotropy theory. And the temporal signal can be interpreted via windowed-FFT or wavelet transformation as a 2D anisotropic power spectrum density $P(k_\perp, k_\parallel)$ (or even 3D depending on the specific turbulence theory one choose to compare to).

Partially due to the stability of the Alfvén mode (see e.g. Hollweg (1971)), the Alfvén speed $V_A = |B|/\sqrt{\mu_0\rho}$ is often considered as the representation of the information propagation speed in solar wind plasma. In the near-Earth solar wind, solar wind speed $U \simeq 400\text{km/s}$ is much larger than the typical Alfvén speed $V_A \simeq 50\text{km/s}$, and hence (B1) is accurate with an error around 10% at 1AU, thereby being the common approach. However, as PSP gets closer to the sun, especially around the Alfvén surface (Kasper et al. 2021) where U becomes comparable to V_A by definition, (B1) needs to be modified. The commonly used modification is that:

$$\vec{k} \cdot (\vec{U} + \vec{V}_A) = 2\pi f \tag{B2}$$

where $\vec{V}_A$ has a scale-dependent direction determined by the local average magnetic field direction, and similarly $\vec{k}$ is assumed to align with $\vec{U} + \vec{V}_A$. This modified TH makes an extremely important assumption: All of the temporal signals in the solar wind measured by PSP are propagating Alfvén waves. This assumption is of course questionable since all types of transients exists in the solar wind: Heliospheric Current Sheets (HCS), Coronal Mass Ejections (CME), and discontinuities (tangential, shocks, etc.). Nevertheless, this assumption can be justified for PSP data with two major reasons: 1. The solar wind measured by PSP around the perihelion (±7 days) is Alfvénic (high $\vec{V}$ and $\vec{B}$ correlation) most of the time ($> 80\%$), signifying unidirectional outward propagating Alfvén waves; 2. For turbulence studies, the large scale transients (HCS or CME) are usually removed prior to statistical analysis in order to make meaningful comparisons with theories.

However, instead of invoking TH and converting the temporal signals into spatial signals, one can resort to a more straightforward approach: make the same assumption that PSP is measuring unidirectional outward propagating Alfvén waves and directly analyze the frequency spectrum compiled from the temporal signals.

B.1. Tranmission of Alfvén Waves

To justify the aforementioned approach, one needs to consider the propagation properties of Alfvén waves in the solar wind which experiences significant expansion and acceleration from the coronal base to PSP. The transmission coefficient of Alfvén waves in the solar wind is defined in terms of the total wave action (quantum) flux for an expanding flux tube starting from the coronal base (Heinemann & Olbert 1980; Velli 1993):

$$S^\pm = \frac{1}{2}\rho\frac{(z^\pm/2)^2}{\omega_0\frac{V_A}{U+V_A}} \cdot (U \pm V_A) \cdot A \tag{B3}$$

where $\vec{z}^\pm = \vec{v} \pm \vec{b}$ is the Elsässer variable, and $\vec{b} = \frac{\delta\vec{B}}{\sqrt{\mu_0\rho}}$ is the normalized magnetic perturbation in the system. Here we defined z^+ as the outward-propagating Alfvén waves and hence S^+ is the wave action density of the outward component, and vice versa for z^- and S^-. A is the cross section area of the flux tube as a function of radial distance, and in the case of spherical expansion $A(R) \propto R^2$. Notably, ω_0 is the launch angular frequency of the wave at the coronal base, and it is doppler shifted to ω_1 in the plasma frame (for simplicity, z^+ will be used as an example):

$$\omega_1 = \omega_0\frac{V_A}{U+V_A} \tag{B4}$$

because from the perspective of the wave in the plasma frame, the source is moving away at the speed of U. And hence here:

$$\frac{1}{2}\rho(z^+/2)^2$$

is the fluctuation energy density of the Alfvén wave packet, and:

$$\frac{1}{2}\rho\frac{(z^+/2)^2}{\omega_1} = \frac{1}{2}\rho\frac{(z^+/2)^2}{\omega_0\frac{V_A}{U+V_A}}$$

is the wave action density of the Alfvén wave packet, which is an adiabatic invariant for a propagating wave when the wavelength is much shorter than the typical spatial scale of the medium (Bretherton 1968; Dewar 1970). This is also

called the wave quantum because it has exactly the same definition as a photon. For a given frequency, if the wave is adiabatic, we can regard the wave packet as a particle, and speed of the particle in inertial frame is the group velocity $U + V_A$, and thus:

$$\frac{1}{2}\rho\frac{(z^+/2)^2}{\omega_0\frac{V_A}{U+V_A}} \cdot (U + V_A) \tag{B5}$$

is the wave action flux density, and together with the cross section area A of the flux tube at a given radial distance R, making (B3) the total wave action flux as a function of R. Evidently, when the outward propagating wave is adiabatic, S^+ is a perfectly conserved quantity, i.e. the total number of 'Alfvénton' being a constant for any given cross section of the flux tube. This is also termed as being WKB (Wentzel-Kramers-Brillouin) (Whang 1973; Hollweg 1990). However, due to the spatial gradient of U, V_A, ρ and A, low frequency waves can become non-WKB and be partially reflected (and partially tunnelled). The transmission problem is then phrased in terms of the WKB value of the total wave action flux, thereby producing a frequency-dependent transmission coefficient profile. The key point to solve the transmission problem of $z^\pm$ is that from the corona base (source) to infinity, the net flux of the outward propagating Alfvén waves is constant:

$$S^+ - S^- = S_\infty \tag{B6}$$

where S_∞ is the total wave action flux at infinity. The transmission coefficient for a given launch angular frequency ω_0 is hence defined as:

$$T = T_\infty/S_0^+ \tag{B7}$$

where S_0^+ is the total wave action flux at the corona base. To solve this problem, one needs to integrate the following equation:

$$-i\omega z^\pm + (\vec{U} \pm \vec{V}_A) \cdot \nabla z^\pm + z^\mp \cdot \nabla(\vec{U} \mp \vec{V}_A) + \frac{1}{2}(z^- - z^+)\nabla \cdot (\vec{V}_A \mp \frac{1}{2}\vec{U}) = 0 \tag{B8}$$

where the ω is the angular frequency of the wave in an inertial frame at distance R. Note that this inertial frame is the same frame as the solar inertial frame, and thus $\omega = \omega_0$, the launch angular frequency of the wave. Intuitively, this can be explained using double doppler shifts with three frames involved: solar inertial frame S_0, solar wind plasma frame P, and the stationary (relative to the sun) spacecraft frame S. In S_0, the frequency of the wave is ω_0. It is doppler shifted to a lower frequency ω_1 in P, shown in (B4), because the wave sources moves away with respective to an observer in the frame. The frequency is then shifted back to ω_0 in S because, for an observer in S, the receiver is moving at U with respect to the source, and hence:

$$\omega = \omega_1\frac{U + V_A}{V_A} = \omega_0 \tag{B9}$$

However, integrating (B8) is quite tricky because one needs to set a boundary condition, but we have no information on the relations between z^+ and z^- either at the corona base or infinity. Luckily, the Alfvén surface where $U = V_A$, acts as a natural singular point in this system, because the z^- equation in (B8) reduces to:

$$-i\omega z^- + \frac{1}{2}(z^- - z^+)\nabla \cdot (\vec{V}_A + \frac{1}{2}\vec{U}) = 0 \tag{B10}$$

and given a radial profile of $V_A(R)$ and $U(R)$, one obtains a linear relation between z^+ and z^- at the Alfvén surface. In addition, the group velocity for the inward waves is zero at the Alfvén surface, and hence the net total wave action flux S_∞ is:

$$S_\infty = S_c^+ - S_c^- = S_c^+ \tag{B11}$$

where $S_c^\pm$ is the total wave action flux for $z^\pm$ at the Alfvén (critical) surface. Now combining (B8), (B10) and (B11), we can integrate the equations for both z^+ and z^- from the Alfvén surface back to the corona base and obtain a
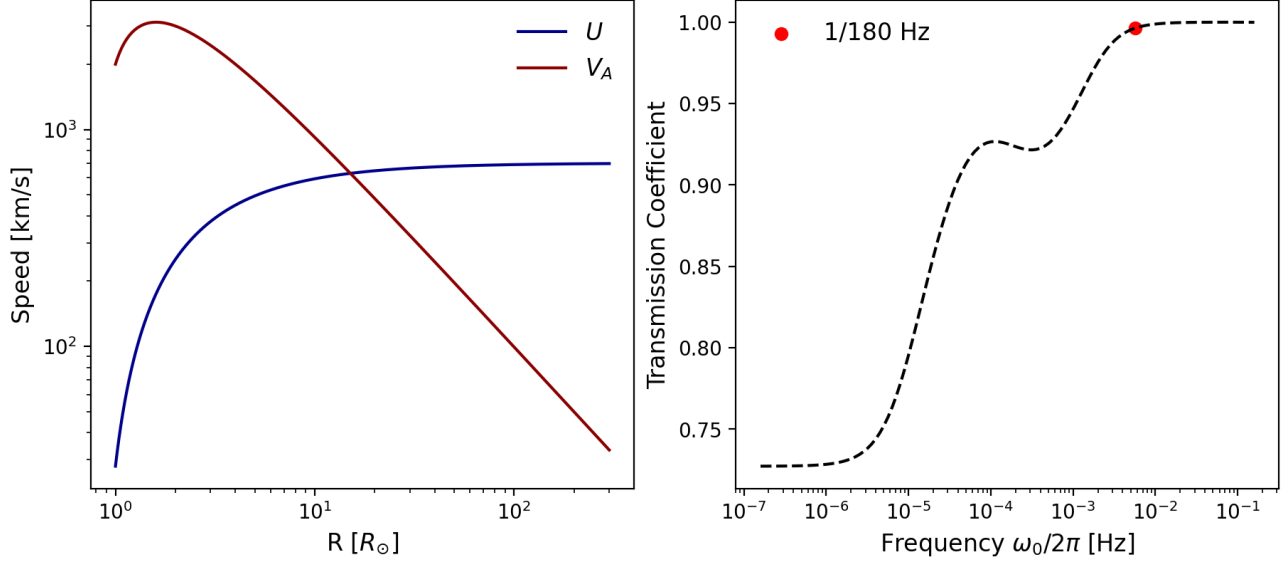
Figure 4. Left: Solar wind and Alfvén speed profile. Right: Transmission coefficient of Alfvén waves as a function of launch frequency.

transmission coefficient profile from the corona base to the Alfvén surface. As an example, here we use the solar wind and Alfvén speed profile from Velli et al. (1991):

$$\rho = \rho_0 \frac{\exp\{-\alpha/2 \cdot [1 - (R_\odot/R)]\}}{\{1 + \beta[(R/R_\odot - 1)]\}^2} \tag{B12}$$

$$V_A = V_{A0} \left(\frac{R_\odot}{R}\right)^2 \left(\frac{\rho_0}{\rho}\right)^{1/2} \tag{B13}$$

$$U = \frac{U_\infty}{\beta^2} \exp(-\alpha/2) \left(\frac{R}{R_\odot}\right)^2 \left(\frac{V_A}{V_{A0}}\right)^2 \tag{B14}$$

where V_{A0} is the initial Alfvén speed at the corona base, U_∞ is the asymptotic solar wind speed at infinity, and α and β are free parameters. To find a typical transmission coefficient for the 3-minute ($\simeq$5.5 mHz) wave, we adopt some reasonable values: $\alpha = 0, \beta = 5, V_{A0} = 2000$km/s, $U_\infty = 700$km/s, and this produces a Alfvén surface at a observational compatible distance of $15.09 R_\odot$. The resulting solar wind and Alfvén speed profile is shown in the left panel of Figure 4, and in the right panel we show the transmission coefficient as a function of launch frequency $f_0 = \omega_0/2\pi$. From the graph we can see that for an Alfvén wave packet with a period of 3 minute, the transmission coefficient from the corona base to the Alfvén surface is 99.6%, very close to perfect transmission. And for the ultra-low frequency waves, asymptotic transmission coefficient is tunnelling value determined solely by the Alfvén speed at the corona base V_{A0} and at the Alfvén (critical) surface V_{Ac}:

$$T_c = 4 \frac{V_{A0} V_{Ac}}{(V_{A0} + V_{Ac})^2} \tag{B15}$$

The transmission is much enhanced compared to the case of static atmosphere with exponential Alfvén speed profile, where the ultra-low frequency waves are completely reflected. Notably, the transmission coefficient value for a 3-minute wave is not sensitive to the specific profile of U and V_A as long as the given profiles are realistic. In addition, for the frequency range that we are dealing with in this study ($f \gtrsim 10^{-4}$ Hz), the transmission coefficient is generally larger than 90%, and hence can be safely considered as quasi-WKB. For more in depth discussion of the transmission problem, please refer to Velli (1993).

B.2. *Doppler Effects*

Through the discussion in the previous section we have shown that for the frequency range we studied in this work, the linear theory dictates a perfect transmission, in other words, negligible modification to the frequency spectrum except

for the systematic decay in energy from WKB evolution. However, PSP is the fastest moving human-made object, and hence especially during the perihelion, doppler effects resulting from the spacecraft movement can be significant. Again, we emphasize our fundamental assumption that PSP is measuring unidirectional outward propagating Alfvén waves, and therefore the doppler effects can be separated into two scenarios (PSP orbit is mostly within the ecliptic plane with very little θ variations): radial velocity of PSP $V_{PSP,r}$ and perpendicular velocity of PSP $V_{PSP,\phi}$.

B.2.1. *Radial Doppler Shift*

Treating the radial doppler shift is trivial, we can simply incorporate the spacecraft velocity in (B9):

$$f = f_1 \frac{U + V_A + V_{PSP,r}}{V_A} = f_0 \frac{U + V_A + V_{PSP,r}}{U + V_A} \tag{B16}$$

where f_0 is the launch frequency, f_1 is the doppler shifted frequency in the solar wind plasma frame, and f is the frequency of the wave in the spacecraft frame. Here we select the sign of $V_{PSP,r}$ to be positive when the spacecraft is moving radially inward. Around perihelion, $V_{PSP,r} \simeq 100$km/s, whereas $U + V_A \gtrsim 1000$km/s, and hence $f/f_0 < 10\%$. To visualize this effect, the radial doppler shift is removed for the coronal hole interval from E12, and the comparison is shown in Figure 5 (b). Obviously the effect makes little change to the raw values of $1/f_{mid}$ and hence we decided to keep the original data of $1/f_{mid}$ in the statistical results shown in Figure 3. In summary, the radial doppler effects from the radial movements of PSP are marginal for all intervals considered in this study.

B.2.2. *Perpendicular Doppler Shift*

The perpendicular doppler shift, on the other hand, is much less straightforward. It is well-known that Alfvén waves are guided by the background field $\vec{B}_0$, and the group velocity is perfectly aligned with $\vec{B}_0$. Consequently, Alfvén waves packets hardly interact with each other in the perpendicular direction in large scales. Therefore, the perturbation of $\delta\vec{B}$ in the ϕ direction is an unknown function of spatial coordinates, which can be expressed as a unknown wavenumber power spectrum density in ϕ direction $P(k_\phi)$. As PSP approaches the perihelion, its velocity $V_{PSP,\phi}$ can reach to around 170km/s, or 100km/s in the Carrington corotating frame. And hence the wavenumber spectrum (spatial signals) can be doppler shifted to frequency spectrum via:

$$2\pi f = k_\phi \cdot V_{PSP,\phi} \tag{B17}$$

The doppler shifted spectrum can then be considered as a "contamination" of the real frequency spectrum of the outward propagating Alfvén waves. Notably, $V_{PSP,\phi}$ change significantly around the perihelion over a relatively small range of radial distance, especially in the solar corotating frame. Assuming a power law dependence $P(k_\phi) \propto k^{-\alpha}$ and $\alpha > 1$, smaller k (larger scales) indicates stronger fluctuation energy. In this scenario, as PSP approaches perihelion, $V_{PSP,\phi}$ increases rapidly, and hence for the same frequency f, it corresponds to progressively smaller k, and hence increasingly higher fluctuation energy. Therefore, the "contamination" grows rapidly as PSP approaches perihelion, and reaches its maximum right at the perihelion. This could be reason why we see an upward trend in $1/f_{mid}$ right at the perihelion for the coronal hole interval from the inbound section of E12 shown in Figure 5 (and similarly for E10 coronal hole shown in Figure 3). Therefore, the actual $1/f_{mid}$ in the upper corona could be closer to 2-minute than 3-minute if the contamination is removed. Nevertheless, we decided to keep the original statistics to maintain reproductivity and generality of our study.

B.3. *Nonlinear Effects: Parametric Decay Instability and Turbulence Cascade*

Based on the discussion in the previous section, we have shown that for the frequency range of interest, the reflection of Alfvén waves are negligible. Therefore, nonlinear effects are necessary in order to change the frequency spectrum of the Alfvén waves. There are two major nonlinear effects that is believed to be significant in the solar wind at PSP distance: parametric decay instability (PDI) and turbulence cascade. However, instead of discussing the details of the two nonlinear effects, one can estimate the propagation time of the Alfvén waves from the corona base to Alfvén surface using the group velocity $U + V_A$. Assuming a radially expanded flux tube (which slightly underestimates the real length of the field line because the plume lines in during solar eclipse clearly show super-radial expansion), the propagation time compiled from the profile in Figure 4 is 1.55 hours, much shorter than the 'age' of plasma estimated from the advection time $\tau_{adv} = R/U$ shown in Figure 3.
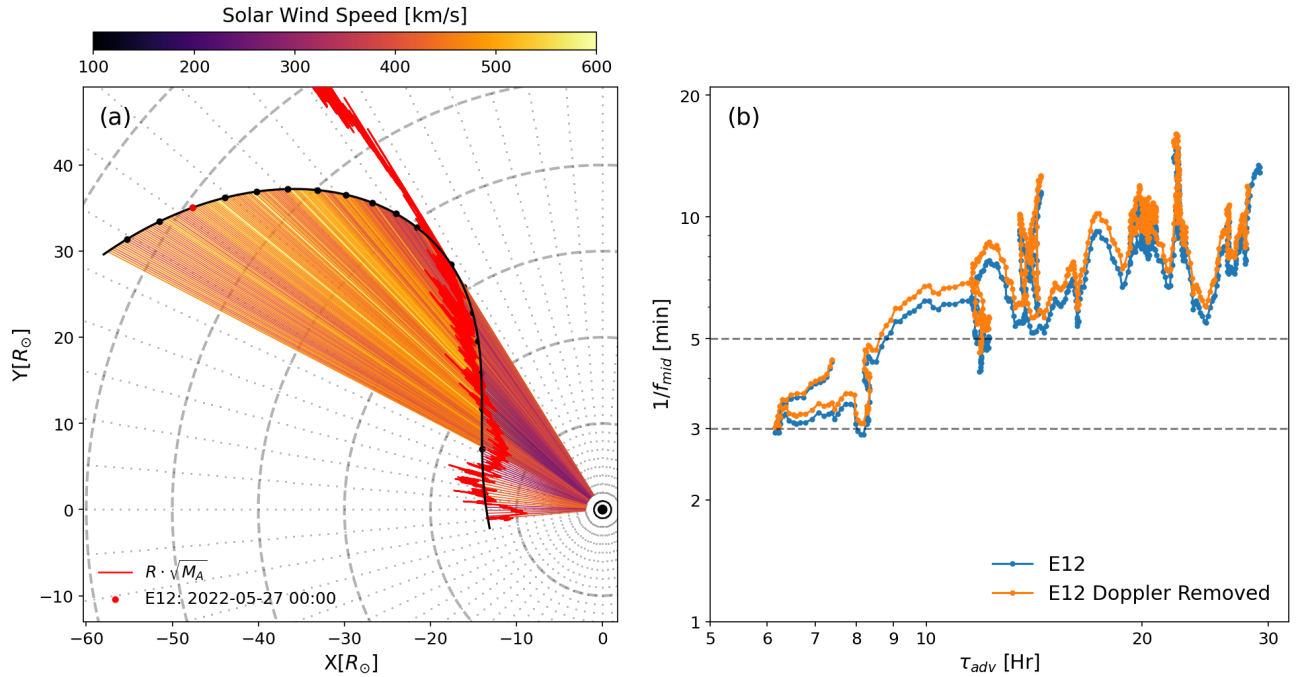
Figure 5. (a) Trajectory of PSP for the inbound section of E12 from 2022-05-26 02:15:00 to 2022-06-01 21:45:00. This interval has confirmed origin from a coronal using PFSS model (Huang et al. 2023c). The black dots on the trajectory are plotted every 8 hours, and the date of the red dot is shown in the legend to indicate the spacecraft's entering direction. The helio-radial lines are colored with locally averaged solar wind speed. The red line is an illustration of Alfvén Mach number $M_A = V_r/V_A$, and is plotted as $R \cdot \sqrt{M_A}$. (b) An illustration of Doppler effects from the spacecraft motion. Blue: $1/f_{mid}$ with doppler effects; Orange: doppler effects are removed.

The main effect of PDI from model (Chandran 2018) is 'spreading' the energy at the bend to lower frequencies through inverse cascade of Alfvén waves. Even though this mechanisms is still being debated, the predicted processes have gained some evidence from recent observations (Davis et al. 2023) and from the supplemental video of this work. A detailed discussion of this mechanism is beyond the scope of this study. Nevertheless, the fact that we identified a systematic collection of the shallow-inertial double power law spectrum around the perihelion indicates that parametric decay instability might not have made significant modification to the spectrum yet when they are captured by PSP. The turbulence cascade, on the other hand, is much slower. We have already provided in depth discussion of this effect in the main text, and thus will be skipped here.

B.4. *Turbulence Anisotropy*

For completeness, here we provide a discussion on the 'sampling-bias' in the turbulence anisotropy. It has been shown in Sioulas et al. (2023a) that the 'parallel' spectrum dominates the large scale (small k) part of the anisotropic PSD. Here the concept of 'parallel' and 'perpendicular' are defined w.r.t. the angle between the local solar wind speed and the scale-dependent background magnetic field. At low frequency (large scale from Taylor Hypothesis), the background field is almost perfectly radial, and hence parallel to the solar wind, and thereby creating a 'sampling-bias' in the anisotropic PSD.

As been discussed in the previous sections, this study choose an alternative yet equal approach: Instead of invoking Taylor Hypothesis and converting the temporal signals into spatial signals, we interpret the temporal signals measured by PSP as it is, and directly analyze the frequency spectrum. Ultimately, the choice between either approaches is dependent on whether one believes that the perturbations in the solar wind are waves or turbulence. Our justification for the prior is the following: The majority of the perturbation energy are carried by the so called switchbacks, or large amplitude spherically polarized Alfvén waves, which are very clearly radially propagating outwards along the quasi-radial background field. It is true that at smaller scales, the waves are guided by the locally perturbed magnetic field, but by definition, these waves are energetically less significant. Additionally, for the perturbations at 3-minute period, at Alfvén surface, it can be translated to 0.26 $R_\odot$ in spatial scale assuming a 1000km/s group velocity. Applying this

spatial scale to the ϕ direction, due to the lack of perpendicular information carrier, we are almost sure that the two signals separated by this distance are causally unrelated. Therefore, following the discussions in the previous section, perturbations created by PSP perpendicular movements at this spatial scales should be considered as 'contamination' to the temporal signals.

C. WINDOW LIMIT

Figure 6 is an illustration of the window limit of 20 minute for the 6 hour window (the dotted dashed line in Figure 3). For a Kolmogorov $f^{-5/3}$ spectrum, the fluctuation power concentrates at the low frequency end. Therefore, the normalized integrated energy (dotted dashed line in Figure 6) grows slowly at high frequencies and quickly at low frequencies. If we similarly ignore the frequency range where more than 50% of points fall out of the Cone of Influence (CoI) of the wavelet transformation (gray area), the resultant frequency range that contains 50% of fluctuation energy (from 25% to 75%) is highlighted with the green area, and the center frequency is $1/f_{mid} = 20$ minute. This frequency can be considered as the saturation frequency because as the solar wind propagates outwards (τ_{adv} and R increases), the low frequency spectral break is known to move to lower frequencies (Tu & Marsch 1993, 1995). And for a fixed 6 hour window, the low frequency break can move well into the grey area, or even fall out of the resolvable frequency range (in this case, $<1/6$Hr$\simeq 10^{-4.3}$Hz). Consequently, the frequency range of interest (right of gray area) is only left with the inertial range, which is often very close to Kolmogorov $f^{-5/3}$ in the solar wind.

The window limit is of course dependent on the window size, and in this case is 6 hour. In this study, we thoroughly scanned the solar wind with windows of different sizes. For shorter window sizes, the window limit become smaller, and hence making it harder to capture the radial evolution of $1/f_{mid}$. On the other hand, longer window can capture the radial evolution nicely, but may fail to resolve the elementary solar wind streams, i.e. tend to mix different streams. This is because PSP retrogrades extremely rapidly at the perihelia, often exceeding 60 deg Carrington Longitude per day (i.e. 2.5 deg/Hr, see e.g. Figure 2(c1)). And hence the *in situ* time series measured at perihelia are often mixtures of very different solar wind streams. For example in Appendix A, the majority of the intervals with clear shallow power law is shorter than 6 hours. From our experience, 6 hour is a good trade-off window size to balance these two effects, and therefore we choose 6 hour window to illustrate our statistical results. Nevertheless, the primary conclusion is not sensitive to the choice of the window size.
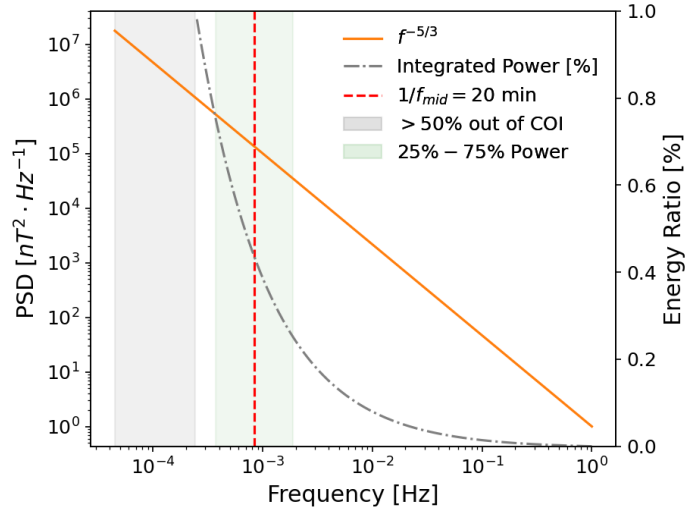
Figure 6. Illustration of the saturation value of $1/f_{mid}$ from a 6 hour window. Orange: Fake Kolmogorov $f^{-5/3}$ spectrum; Dotted dashed: Normalized integrated power of $f^{-5/3}$, twin axis; Gray area: Frequency range where $>50\%$ of points are out of the Cone of Influence; Green area: frequency range that contains 50% of fluctuation energy (from 25% to 75%).

D. MOVEMENT OF THE LOW FREQUENCY SPECTRAL BREAK IN EXPANDING SOLAR WIND

Suppose a well-developed turbulence whose power spectrum consists of two parts:

$$P(f,\tau) = \begin{cases} C_0(\tau)f^{-\alpha_0}, & f \leq f_c(\tau) \\ C_1(\tau)f^{-\alpha_1}, & f \geq f_c(\tau) \end{cases} \tag{D18}$$

Where τ is the "age" of the turbulence starting from a reference point, satisfying that $\tau \gg 1/f_{min}$. f_{min} is the lowest frequency that is considered credible in the spectrum due to the Cone of Influence (CoI), and for a 6-hour fixed window, it is about 80 minutes. Obviously, there should be:

$$C_0(\tau)f_c^{-\alpha_0} = C_1(\tau)f_c^{-\alpha_1} \tag{D19}$$

at any given moment. Here we have assumed that the energy containing range is decaying due to the solar wind expansion, otherwise $C_0(\tau)$ should be a constant.

The total energy in the system at moment t is:

$$\mathcal{E}(\tau) = \int_0^{+\infty} P(f,\tau)df = \int_0^{f_c(\tau)} C_0(\tau)f^{-\alpha_0}df + \int_{f_c(\tau)}^{+\infty} C_1(\tau)f^{-\alpha_1}df \tag{D20}$$

At a later time $t + \Delta\tau$, the total energy is:

$$\begin{aligned}
\mathcal{E}(\tau + \Delta\tau) &= \int_0^{+\infty} P(f,\tau+\Delta\tau)df \\
&= \int_0^{f_c(\tau+\Delta\tau)} C_0(\tau+\Delta\tau)f^{-\alpha_0}df + \int_{f_c(\tau+\Delta\tau)}^{+\infty} C_1(\tau+\Delta\tau)f^{-\alpha_1}df \\
&\simeq \int_0^{f_c(\tau)+\Delta f_c} \left[C_0(\tau) + \frac{dC_0}{dt}\Delta\tau\right] f^{-\alpha_0}df + \int_{f_c(\tau)+\Delta f_c}^{+\infty} \left[C_1(\tau) + \frac{dC_1}{dt}\Delta\tau\right] f^{-\alpha_1}df
\end{aligned} \tag{D21}$$

From equation (D19), we can see that:

$$\frac{dC_1}{dt} = \frac{dC_0}{dt}f_c^{\Delta\alpha} + \Delta\alpha C_0 f_c^{\Delta\alpha-1}\frac{df_c}{dt} \tag{D22}$$

where $\Delta\alpha = \alpha_1 - \alpha_0$. Here the first r.h.s term is the change of the inertial range energy due to the solar wind expansion, and the second term is the change of the inertial range energy due to the movement of the low frequency spectral break f_c. Thus, we get:

$$\begin{aligned}
\mathcal{E}(\tau + \Delta\tau) &= \int_0^{f_c(\tau)+\Delta f_c} C_0 f^{-\alpha_0}df + \int_{f_c(\tau)+\Delta f_c}^{+\infty} C_1 f^{-\alpha_1}df \\
&+ \Delta\alpha C_0 f_c^{\Delta\alpha-1}\frac{df_c}{dt}\Delta\tau \cdot \int_{f_c(\tau)+\Delta f_c}^{+\infty} f^{-\alpha_1}df \\
&+ \frac{dC_0}{dt}\Delta\tau \left[\int_0^{f_c(\tau)+\Delta f_c} f^{-\alpha_0}df + f_c^{\Delta\alpha} \cdot \int_{f_c(\tau)+\Delta f_c}^{+\infty} f^{-\alpha_1}df\right]
\end{aligned} \tag{D23}$$

It is obvious that the first line is equal to $\mathcal{E}(\tau)$. The second line is the change of total energy due to the movement of the low frequency spectral break due to turbulence dissipation. The third line is the change of total energy due to solar wind expansion. We can hence write the energy dissipation rate as $\epsilon(\tau)$:

$$\begin{aligned}
-\epsilon(\tau) = \frac{\mathcal{E}(\tau + \Delta\tau) - \mathcal{E}(\tau)}{\Delta\tau} &= \Delta\alpha C_0 f_c^{\Delta\alpha-1}\frac{df_c}{dt} \cdot \int_{f_c(\tau)+\Delta f_c}^{\infty} f^{-\alpha_1}df \\
&\approx \left(\frac{\alpha_1 - \alpha_0}{\alpha_1 - 1}\right) C_0 f_c^{-\alpha_0}\frac{df_c}{dt}
\end{aligned} \tag{D24}$$

One may use (D24) to evaluate the energy cascade rate $\epsilon(\tau)$ from the change of $f_c(\tau)$ over time.

REFERENCES

Adhikari, L., Zank, G. P., Zhao, L.-L., et al. 2020, The Astrophysical Journal Supplement Series, 246, 38, doi: 10.3847/1538-4365/ab5852

Alazraki, G., & Couturier, P. 1971, Astronomy and Astrophysics, Vol. 13, p. 380 (1971), 13, 380

Angelopoulos, V., Cruce, P., Drozdov, A., et al. 2019, Space Science Reviews, 215, 9, doi: 10.1007/s11214-018-0576-4

Badman, S. T., Bale, S. D., Oliveros, J. C. M., et al. 2020, The Astrophysical Journal Supplement Series, 246, 23, doi: 10.3847/1538-4365/ab4da7

Badman, S. T., Riley, P., Jones, S. I., et al. 2023, Journal of Geophysical Research: Space Physics, 128, e2023JA031359, doi: 10.1029/2023JA031359

Bak, P., Tang, C., & Wiesenfeld, K. 1987, Physical Review Letters, 59, 381, doi: 10.1103/PhysRevLett.59.381

Bale, S. D., Goetz, K., Harvey, P. R., et al. 2016, ßr, 204, 49, doi: 10.1007/s11214-016-0244-5

Bale, S. D., Badman, S. T., Bonnell, J. W., et al. 2019, Nature, 1, doi: 10.1038/s41586-019-1818-7

Bale, S. D., Horbury, T. S., Velli, M., et al. 2021, The Astrophysical Journal, 923, 174, doi: 10.3847/1538-4357/ac2d8c

Bale, S. D., Drake, J. F., McManus, M. D., et al. 2023, Nature, 618, 252, doi: 10.1038/s41586-023-05955-3

Banerjee, D., Krishna Prasad, S., Pant, V., et al. 2021, Space Science Reviews, 217, 76, doi: 10.1007/s11214-021-00849-0

Barnes, A., & Hollweg, J. V. 1974, Journal of Geophysical Research, 79, 2302, doi: 10.1029/JA079i016p02302

Bavassano, B., Dobrowolny, M., Fanfoni, G., Mariani, F., & Ness, N. F. 1982, Solar Physics, 78, 373, doi: 10.1007/BF00151617

Belcher, J. W. 1971, Astrophysical Journal, vol. 168, p.509, doi: 10.1086/151105

Belcher, J. W., & Davis, L. 1971, Journal of Geophysical Research, 76, 3534, doi: 10.1029/JA076i016p03534

Belcher, J. W., & Olbert, S. 1975, The Astrophysical Journal, 200, 369

Bemporad, A., Matthaeus, W. H., & Poletto, G. 2008, The Astrophysical Journal, 677, L137, doi: 10.1086/588093

Bizien, N., Wit, T. D. d., Froment, C., et al. 2023, The Astrophysical Journal, 958, 23, doi: 10.3847/1538-4357/acf99a

Bogdan, T. J., Hansteen, M. C. V., McMurry, A., et al. 2003, The Astrophysical Journal, 599, 626, doi: 10.1086/378512

Bretherton, F. P. 1968, Proceedings of the Royal Society of London. Series A. Mathematical and Physical Sciences, 302, 529, doi: 10.1098/rspa.1968.0034

Bruno, R., & Carbone, V. 2013, Living Reviews in Solar Physics, 10, 2, doi: 10.12942/lrsp-2013-2

Bruno, R., Telloni, D., Sorriso-Valvo, L., et al. 2019, Astronomy & Astrophysics, 627, A96, doi: 10.1051/0004-6361/201935841

Burlaga, L. F., & Goldstein, M. L. 1984, Journal of Geophysical Research: Space Physics, 89, 6813, doi: 10.1029/JA089iA08p06813

Cally, P. 2000, Solar Physics, 192, 395, doi: 10.1023/A:1005213002513

Cally, P. S. 2012, Solar Physics, 280, 33, doi: 10.1007/s11207-012-0052-3

—. 2017, Monthly Notices of the Royal Astronomical Society, 466, 413, doi: 10.1093/mnras/stw3215

Cally, P. S., & Bogdan, T. J. 1997, The Astrophysical Journal, 486, L67, doi: 10.1086/310833

Cally, P. S., & Hansen, S. C. 2011, The Astrophysical Journal, 738, 119, doi: 10.1088/0004-637X/738/2/119

Chandran, B. D. G. 2018, Journal of Plasma Physics, 84, doi: 10.1017/S0022377818000016

Chen, C. H. K. 2022, Nature Astronomy, 6, 637, doi: 10.1038/s41550-022-01716-w

Chen, C. H. K., Bale, S. D., Bonnell, J. W., et al. 2020, The Astrophysical Journal Supplement Series, 246, 53, doi: 10.3847/1538-4365/ab60a3

Cranmer, S. R., & Ballegooijen, A. A. v. 2005, The Astrophysical Journal Supplement Series, 156, 265, doi: 10.1086/426507

Crouch, A., & Cally, P. 2003, Solar Physics, 214, 201, doi: 10.1023/A:1024247617255

Davis, N., Chandran, B. D. G., Bowen, T. A., et al. 2023, The Astrophysical Journal, 950, 154, doi: 10.3847/1538-4357/acd177

De Pontieu, B., McIntosh, S. W., Carlsson, M., et al. 2007, Science, 318, 1574, doi: 10.1126/science.1151747

Denskat, K. U., & Neubauer, F. M. 1982, Journal of Geophysical Research: Space Physics, 87, 2215, doi: 10.1029/JA087iA04p02215

Dewar, R. L. 1970, Physics of Fluids, 13, 2710, doi: 10.1063/1.1692854

Dmitruk, P., Mininni, P. D., Pouquet, A., Servidio, S., & Matthaeus, W. H. 2011, Physical Review E, 83, 066318, doi: 10.1103/PhysRevE.83.066318

Drake, J. F., Agapitov, O., Swisdak, M., et al. 2021, Astronomy & Astrophysics, 650, A2

Dudok de Wit, T., Krasnoselskikh, V. V., Bale, S. D., et al. 2020, The Astrophysical Journal Supplement Series, 246, 39, doi: 10.3847/1538-4365/ab5853

Dunn, C., Bowen, T., Mallet, A., Badman, S., & Bale, S. 2023, Effect of Spherical Polarization on the Magnetic Spectrum of the Solar Wind, arXiv, doi: 10.48550/arXiv.2305.09763

Fleck, B., & Schmitz, F. 1991, Astronomy and Astrophysics (ISSN 0004-6361), vol. 250, no. 1, Oct. 1991, p. 235-244., 250, 235

Foukal, P. 2004, Solar astrophysics, 2nd edn. (Weinheim: Wiley-VCH)

Fox, N. J., Velli, M. C., Bale, S. D., et al. 2016, Space Science Reviews, 204, 7, doi: 10.1007/s11214-015-0211-6

Gringauz, K. I., Bezrukikh, V. V., Ozerov, V. D., & Rybchinskii, R. E. 1962, Planetary and Space Science, 9, 103, doi: 10.1016/0032-0633(62)90180-0

Hansen, S. C., & Cally, P. S. 2012, The Astrophysical Journal, 751, 31, doi: 10.1088/0004-637X/751/1/31

Hansteen, V. H., & Leer, E. 1995, Journal of Geophysical Research: Space Physics, 100, 21577, doi: 10.1029/95JA02300

Hansteen, V. H., & Velli, M. 2012, Space Science Reviews, 172, 89, doi: 10.1007/s11214-012-9887-z

Harris, C. R., Millman, K. J., van der Walt, S. J., et al. 2020, Nature, 585, 357, doi: 10.1038/s41586-020-2649-2

Heinemann, M., & Olbert, S. 1980, Journal of Geophysical Research: Space Physics, 85, 1311, doi: 10.1029/JA085iA03p01311

Hollweg, J. V. 1971, Journal of Geophysical Research (1896-1977), 76, 5155, doi: 10.1029/JA076i022p05155

—. 1990, Journal of Geophysical Research: Space Physics, 95, 14873, doi: 10.1029/JA095iA09p14873

Huang, J., Kasper, J. C., Fisk, L. A., et al. 2023a, The Astrophysical Journal, 952, 33, doi: 10.3847/1538-4357/acd17e

Huang, Z., Shi, C., Sioulas, N., & Velli, M. 2022, The Astrophysical Journal, 935, 60, doi: 10.3847/1538-4357/ac74c5

Huang, Z., Sioulas, N., Shi, C., et al. 2023b, The Astrophysical Journal Letters, 950, L8, doi: 10.3847/2041-8213/acd7f2

Huang, Z., Shi, C., Velli, M., et al. 2023c, doi: 10.48550/ARXIV.2312.08669

Hunter, J. D. 2007, Computing in Science & Engineering, 9, 90, doi: 10.1109/MCSE.2007.55

Jagarlamudi, V. K., Raouafi, N. E., Bourouaine, S., et al. 2023, The Astrophysical Journal Letters, 950, L7, doi: 10.3847/2041-8213/acd778

Jess, D. B., Mathioudakis, M., Erdélyi, R., et al. 2009, Science, 323, 1582, doi: 10.1126/science.1168680

Jess, D. B., Moortel, I. D., Mathioudakis, M., et al. 2012, The Astrophysical Journal, 757, 160, doi: 10.1088/0004-637X/757/2/160

Jess, D. B., Morton, R. J., Verth, G., et al. 2015, Space Science Reviews, 190, 103, doi: 10.1007/s11214-015-0141-3

Kasper, J. C., Bale, S. D., Belcher, J. W., et al. 2019, Nature, 576, 228

Kasper, J. C., Klein, K. G., Lichko, E., et al. 2021, Physical Review Letters, 127, 255101, doi: 10.1103/PhysRevLett.127.255101

Keshner, M. 1982, Proceedings of the IEEE, 70, 212, doi: 10.1109/PROC.1982.12282

Khomenko, E., & Cally, P. S. 2012, The Astrophysical Journal, 746, 68, doi: 10.1088/0004-637X/746/1/68

—. 2019, The Astrophysical Journal, 883, 179, doi: 10.3847/1538-4357/ab3d28

Kruparova, O., Krupar, V., Szabo, A., Pulupa, M., & Bale, S. D. 2023, The Astrophysical Journal, 957, 13, doi: 10.3847/1538-4357/acf572

Kuniyoshi, H., Shoda, M., Morton, R. J., & Yokoyama, T. 2023, doi: 10.48550/ARXIV.2311.16461

Kuridze, D., & Zaqarashvili, T. 2008, Journal of Atmospheric and Solar-Terrestrial Physics, 70, 351, doi: 10.1016/j.jastp.2007.08.059

Lam, S. K., Pitrou, A., & Seibert, S. 2015, in Proceedings of the Second Workshop on the LLVM Compiler Infrastructure in HPC (Austin Texas: ACM), 1–6, doi: 10.1145/2833157.2833162

Larosa, A., Chen, C. H. K., McIntyre, J. R., & Jagarlamudi, V. K. 2023, The relation between magnetic switchbacks and turbulence in the inner heliosphere, arXiv, doi: 10.48550/arXiv.2312.16521

Leer, E., & Holzer, T. E. 1980, Journal of Geophysical Research: Space Physics, 85, 4681, doi: 10.1029/JA085iA09p04681

Magyar, N., & Doorsselaere, T. V. 2022, The Astrophysical Journal, 938, 98, doi: 10.3847/1538-4357/ac8b81

Mandal, S., Chitta, L. P., Antolin, P., et al. 2022, Astronomy & Astrophysics, 666, L2, doi: 10.1051/0004-6361/202244403

Mathioudakis, M., Jess, D. B., & Erdélyi, R. 2013, Space Science Reviews, 175, 1, doi: 10.1007/s11214-012-9944-7

Matteini, L., Horbury, T. S., Neugebauer, M., & Goldstein, B. E. 2014, Geophysical Research Letters, 41, 259, doi: 10.1002/2013GL058482

Matteini, L., Stansby, D., Horbury, T. S., & Chen, C. H. K. 2018, The Astrophysical Journal, 869, L32, doi: 10.3847/2041-8213/aaf573

Matteini, L., Tenerani, A., Landi, S., et al. 2024, Physics of Plasmas, 31, 032901, doi: 10.1063/5.0177754

Matthaeus, W. H. 2021, Physics of Plasmas, 28, 032306, doi: 10.1063/5.0041540

Matthaeus, W. H., Breech, B., Dmitruk, P., et al. 2007, The Astrophysical Journal, 657, L121, doi: 10.1086/513075

Matthaeus, W. H., & Goldstein, M. L. 1986, Physical Review Letters, 57, 495, doi: 10.1103/PhysRevLett.57.495

McComas, D. J., Barraclough, B. L., Funsten, H. O., et al. 2000, Journal of Geophysical Research: Space Physics, 105, 10419, doi: 10.1029/1999JA000383

McComas, D. J., Velli, M., Lewis, W. S., et al. 2007, Reviews of Geophysics, 45, doi: 10.1029/2006RG000195

McIntyre, J. R., Chen, C. H., & Larosa, A. 2023, The Astrophysical Journal, 957, 111. https://iopscience.iop.org/article/10.3847/1538-4357/acf3dd/meta

Meyrand, R., Squire, J., Mallet, A., & Chandran, B. D. G. 2023, Reflection-driven turbulence in the super-Alfv\'enic solar wind, arXiv. http://arxiv.org/abs/2308.10389

Montroll, E. W., & Shlesinger, M. F. 1982, Proceedings of the National Academy of Sciences of the United States of America, 79, 3380, doi: 10.1073/pnas.79.10.3380

Morton, R. J., Sharma, R., Tajfirouze, E., & Miriyala, H. 2023, Reviews of Modern Plasma Physics, 7, 17, doi: 10.1007/s41614-023-00118-3

Morton, R. J., Tomczyk, S., & Pinto, R. F. 2016, The Astrophysical Journal, 828, 89, doi: 10.3847/0004-637X/828/2/89

Morton, R. J., Verth, G., Fedun, V., Shelyag, S., & Erdélyi, R. 2013, The Astrophysical Journal, 768, 17, doi: 10.1088/0004-637X/768/1/17

Morton, R. J., Verth, G., Jess, D. B., et al. 2012, Nature Communications, 3, 1315, doi: 10.1038/ncomms2324

Morton, R. J., Weberg, M. J., & McLaughlin, J. A. 2019, Nature Astronomy, 3, 223, doi: 10.1038/s41550-018-0668-9

Mozer, F. S., Bale, S. D., Bonnell, J. W., et al. 2021, The Astrophysical Journal, 919, 60, doi: 10.3847/1538-4357/ac110d

Neugebauer, M., & Snyder, C. W. 1966, Journal of Geophysical Research (1896-1977), 71, 4469, doi: 10.1029/JZ071i019p04469

Panasenco, O., Velli, M., D'Amicis, R., et al. 2020, The Astrophysical Journal Supplement Series, 246, 54, doi: 10.3847/1538-4365/ab61f4

Parker, E. N. 1958, The Astrophysical Journal, 128, 664, doi: 10.1086/146579

—. 1965, Space Science Reviews, 4, 666, doi: 10.1007/BF00216273

—. 1991, The Astrophysical Journal, 372, 719, doi: 10.1086/170015

Raouafi, N. E., Matteini, L., Squire, J., et al. 2023, Space Science Reviews, 219, 8, doi: 10.1007/s11214-023-00952-4

Rasca, A. P., Farrell, W. M., MacDowall, R. J., Bale, S. D., & Kasper, J. C. 2021, The Astrophysical Journal, 916, 84, doi: 10.3847/1538-4357/ac079f

Réville, V., Tenerani, A., & Velli, M. 2018, The Astrophysical Journal, 866, 38, doi: 10.3847/1538-4357/aadb8f

Rieutord, M., Roudier, T., Rincon, F., et al. 2010, Astronomy & Astrophysics, 512, A4, doi: 10.1051/0004-6361/200913303

Rosenthal, C. S., Bogdan, T. J., Carlsson, M., et al. 2002, The Astrophysical Journal, 564, 508, doi: 10.1086/324214

Shi, C. ., Velli, M., Bale, S. D., et al. 2022a, Physics of Plasmas, 29, 122901, doi: 10.1063/5.0124703

Shi, C., Velli, M., Panasenco, O., et al. 2021, Astronomy & Astrophysics, 650, A21, doi: 10.1051/0004-6361/202039818

Shi, C., Panasenco, O., Velli, M., et al. 2022b, The Astrophysical Journal, 934, 152, doi: 10.3847/1538-4357/ac7c11

Shoda, M., Chandran, B. D. G., & Cranmer, S. R. 2021, The Astrophysical Journal, 915, 52, doi: 10.3847/1538-4357/abfdbc

Shrivastav, A. K., Pant, V., Berghmans, D., et al. 2023, doi: 10.48550/ARXIV.2304.13554

Sioulas, N., Huang, Z., Velli, M., et al. 2022, The Astrophysical Journal, 934, 143, doi: 10.3847/1538-4357/ac7aa2

Sioulas, N., Velli, M., Huang, Z., et al. 2023a, The Astrophysical Journal, 951, 141. https://iopscience.iop.org/article/10.3847/1538-4357/acc658/meta

Sioulas, N., Huang, Z., Shi, C., et al. 2023b, The Astrophysical Journal Letters, 943, L8, doi: 10.3847/2041-8213/acaeff

Spruit, H. C., & Bogdan, T. J. 1992, The Astrophysical Journal, 391, L109, doi: 10.1086/186409

Squire, J., Chandran, B. D. G., & Meyrand, R. 2020, The Astrophysical Journal, 891, L2, doi: 10.3847/2041-8213/ab74e1

Taylor, G. I. 1938, Proceedings of the Royal Society of London Series A, 164, 476, doi: 10.1098/rspa.1938.0032

Tenerani, A., Sioulas, N., Matteini, L., et al. 2021, The Astrophysical Journal Letters, 919, L31, doi: 10.3847/2041-8213/ac2606

Tenerani, A., Velli, M., Matteini, L., et al. 2020, The Astrophysical Journal Supplement Series, 246, 32, doi: 10.3847/1538-4365/ab53e1

22

Tian, H., DeLuca, E. E., Cranmer, S. R., et al. 2014, Science, 346, 1255711, doi: 10.1126/science.1255711

Toth, G., Velli, M., & Holst, B. v. d. 2023, The Astrophysical Journal, 957, 95, doi: 10.3847/1538-4357/acfd91

Tsurutani, B. T., Ho, C. M., Arballo, J. K., et al. 1997, Plasma Physics and Controlled Fusion, 39, A237, doi: 10.1088/0741-3335/39/5A/022

Tu, C.-Y., & Marsch, E. 1993, Journal of Geophysical Research: Space Physics, 98, 1257, doi: 10.1029/92JA01947

Tu, C. Y., & Marsch, E. 1995, Space Science Reviews, 73, 1, doi: 10.1007/BF00748891

Ulrich, R. K. 1970, The Astrophysical Journal, 162, 993, doi: 10.1086/150731

Unti, T. W. J., & Neugebauer, M. 1968, The Physics of Fluids, 11, 563, doi: 10.1063/1.1691953

Van Doorsselaere, T., Srivastava, A. K., Antolin, P., et al. 2020, Space Science Reviews, 216, 140, doi: 10.1007/s11214-020-00770-y

Velli, M. 1993, Astronomy and Astrophysics, 270, 304. https://ui.adsabs.harvard.edu/abs/1993A&A...270..304V

Velli, M., Grappin, R., & Mangeney, A. 1989, Physical Review Letters, 63, 1807, doi: chan

—. 1991, Geophysical & Astrophysical Fluid Dynamics, 62, 101, doi: 10.1080/03091929108229128

Velli, M., Pucci, F., Rappazzo, F., & Tenerani, A. 2015, Philosophical Transactions of the Royal Society A: Mathematical, Physical and Engineering Sciences, 373, 20140262, doi: 10.1098/rsta.2014.0262

Verdini, A., Grappin, R., Pinto, R., & Velli, M. 2012, The Astrophysical Journal, 750, L33, doi: 10.1088/2041-8205/750/2/L33

Virtanen, P., Gommers, R., Oliphant, T. E., et al. 2020, Nature Methods, 17, 261, doi: 10.1038/s41592-019-0686-2

Whang, Y. C. 1973, Journal of Geophysical Research, 78, 7221, doi: 10.1029/JA078i031p07221

Wu, H., Tu, C., Wang, X., He, J., & Yang, L. 2020, The Astrophysical Journal Letters, 904, L8, doi: 10.3847/2041-8213/abc5b6

Wu, H., Tu, C., Wang, X., et al. 2021a, The Astrophysical Journal, 912, 84, doi: 10.3847/1538-4357/abf099

Wu, H., Tu, C., Wang, X., & Yang, L. 2021b, The Astrophysical Journal, 922, 92, doi: 10.3847/1538-4357/ac3331

Zank, G. P., Zhao, L.-L., Adhikari, L., et al. 2022, The Astrophysical Journal Letters, 926, L16, doi: 10.3847/2041-8213/ac51da

Zhang, J., Huang, S. Y., Yuan, Z. G., et al. 2022, The Astrophysical Journal, 937, 70, doi: 10.3847/1538-4357/ac8c34

Zhong, S., Nakariakov, V. M., Kolotkov, D. Y., et al. 2023, Nature Communications, 14, 5298, doi: 10.1038/s41467-023-41029-8